Microtubule poleward flux promotes chromosome centering on the spindle

Patrik Risteski[1#], Mihaela Jagrić[1#], Domagoj Božan[2#], Agneza Bosilj[2], Nenad Pavin[2*], Iva M. Tolić[1*]

[1]Division of Molecular Biology, Ruđer Bošković Institute, Bijenička cesta 54, 10000 Zagreb, Croatia
[2]Department of Physics, Faculty of Science, University of Zagreb, Bijenička cesta 32, 10000 Zagreb, Croatia

[#]These authors contributed equally to this work.
[*]Corresponding authors: I.M.T. (tolic@irb.hr), N.P. (npavin@phy.hr)

ABSTRACT

Chromosome alignment at the spindle equator during metaphase is the most remarkable feature of mitosis, which promotes proper chromosome segregation and depends on the forces exerted at the plus end of kinetochore microtubules and polar ejection forces. However, forces arising from lateral mechanical coupling of kinetochore fibers with non-kinetochore microtubules play a role in chromosome alignment, but the mechanism is unclear. Here we introduce a poleward flux-driven centering model that relies on the interaction between bridging and k-fibers, where the pulling forces exerted by k-fibers onto the kinetochores increase with the overlap length and flux velocity difference between k-fibers and bridging microtubules. To test this model, we develop a speckle microscopy assay to measure the poleward flux of individual microtubules in human spindles and show that bridging microtubules undergo poleward flux at a higher rate than kinetochore microtubules. Depletion of the microtubule coupler NuMa increased the difference in the flux velocity of kinetochore and bridging microtubules, suggesting that sliding forces from the bridging fiber are transmitted largely through NuMa onto the associated kinetochore fibers. Depletions of Kif18A/kinesin-8 and/or Kif4A/kinesin-4 increased the flux velocity of kinetochore fibers up to the velocity of bridging fibers, due to the increased coupling resulting from the extended antiparallel overlap regions. We found severe kinetochore misalignment after combining Kif18A depletion with Kif4A and/or PRC1 depletion, suggesting that forces within the bridging fiber have a centering effect on the kinetochores. We propose that lateral length-dependent sliding forces that the bridging fiber exerts onto kinetochore fibers drive the movement of kinetochores towards the spindle center, thereby promoting chromosome alignment.

INTRODUCTION

Chromosome alignment at the spindle equator in metaphase is a hallmark of mitosis and is important for proper completion of mitosis (Fonseca et al., 2019; Maiato et al., 2017). According to the prevailing view, kinetochore alignment is maintained by the forces exerted at the tips of kinetochore fibers (k-fibers) (Armond et al., 2015; Stumpff et al., 2008), with contribution of polar ejection forces acting on chromosome arms (Stumpff et al., 2012; Wandke et al., 2012). However, k-fibers are not isolated from other microtubules in the spindle, but mechanically coupled with non-kinetochore microtubules (McDonald et al., 1992; O'Toole et al., 2020) and other k-fibers (Vladimirou et al., 2013). In the central part of the spindle, a pair of sister k-fibers interacts with a bundle of antiparallel interpolar microtubules termed bridging fiber, which are crosslinked by PRC1 (Kajtez et al., 2016; Polak et al., 2017). Optogenetic experiments have shown that bridging fibers promote kinetochore alignment (Jagrić et al., 2021). Yet, the mechanism how these non-kinetochore microtubules regulate kinetochore positioning is still unclear.

Kinetochore alignment was also studied theoretically and several mechanisms were proposed. Earlier theories propose a major centering force described by a function representing a polar ejection force (Joglekar and Hunt, 2002). This force, along with the dynamic instability of microtubules, is used to explain the movement of kinetochores. Similarly, kinetochore alignment was studied by models that describe polar ejection force together with collective motor forces as well as microtubule polymerization and depolymerization (Civelekoglu-Scholey et al., 2006). Theoretical studies that describe kinetochore centering in small yeast cells predominantly include length-dependent microtubule dynamics, which are regulated by the amount of kinesin-5 or kinesin-8 motors (Gardner et al., 2008; Mary et al., 2015; Gergley et al., 2016; Klemm et al., 2018).

K-fibers undergo poleward flux, a conveyor belt-like movement in which the whole k-fiber is being transported towards the pole while its minus ends depolymerize and plus ends polymerize (Forer, 1965; Hamaguchi et al., 1987; Hiramoto and Izutsu, 1977; Mitchison, 1989). Poleward flux is regulated by several motor proteins, including Kif2a/kinesin-13 that depolymerizes microtubule minus ends at the spindle poles (Ganem et al., 2005; Rogers et al., 2004). A recent comprehensive study showed that flux is driven by CENP-E/kinesin-7, Kif4A/kinesin-4, Eg5/kinesin-5, and Kif15/kinesin-12 (Steblyanko et al., 2020).

Poleward flux is typically studied by using photoactivation, a method that was used for the first demonstration of this process (Mitchison, 1989). In tubulin photoactivation experiments, all the microtubules within the illuminated region are photoactivated, thus the movements of kinetochore and non-kinetochore microtubules cannot be distinguished. Given that kinetochore microtubules provide the strongest tubulin signal in spindles of mammalian somatic cells (Mitchison, 1989), the photoactivated spots are interpreted as belonging to kinetochore fibers. However, it remains unclear whether other spindle microtubules experience flux, how the fluxes

of different microtubule classes are related, and how they affect chromosome alignment.

In this study we introduce a flux-driven centering model that relies on the interaction between bridging and k-fibers. This model describes a centering mechanism based on pulling forces exerted by k-fibers onto the kinetochores. These forces increase with the overlap length and velocity difference, both referring to the relationship between k-fibers and bridging microtubules. To test this model, we developed a speckle microscopy assay and measured the movements of individual microtubules within the spindle of human cells, which allowed us to uncover that bridging microtubules undergo flux during metaphase at a rate higher that kinetochore microtubules. Sliding forces from the bridging fiber are transmitted to the k-fiber in a manner dependent on the coupling between bridging and k-fibers. We show that k-fibers flux slower when this coupling is weakened such as after depletion of NuMa, whereas the k-fiber flux speeds up when the coupling is stronger such as after depletion of Kif18A and/or Kif4A, which results in larger overlaps. Our results suggest a model in which lateral length-dependent sliding forces that the bridging fiber exerts onto k-fibers promote the movement of kinetochores towards the spindle center.

RESULTS

Model for chromosome centering based on microtubule poleward flux

To explore the idea that microtubule poleward flux promotes kinetochore centering, we introduce a "flux-driven centering" model in which k-fibers laterally interact with bridging microtubules (**Fig. 1 A**; **Methods**). The central idea of our theoretical approach is that pulling forces exerted by k-fibers on the kinetochores are proportional to the length of their overlap with bridging microtubules. Our aim is to explore the basic concepts of how this new mechanism works to center a kinetochore that is off-centered, and what features of the spindle are crucial for efficient centering. Thus, our model is based on a simple one-dimensional geometry and does not include other centering mechanism that also operate in a real spindle.

How does this model lead to kinetochore centering? A key feature of the model is that motor proteins accumulate in the antiparallel overlaps between k-fibers and bridging microtubules, where they generate sliding forces that drive the poleward flux of k-fibers. The number of accumulated motors is proportional to the overlap length and when kinetochores are off-centered a difference in the number of motors on the two k-fibers leads to a centering force (**Fig. 1 A**). Motors are also present within the antiparallel overlap between bridging microtubules, where they balance the forces on k-fibers and drive poleward flux of bridging microtubules. Parallel overlaps between k-fibers and bridging microtubules are linked by passive crosslinkers, which help to transmit the sliding forces from the bridging microtubules to the k-fibers. Forces exerted by passive crosslinkers are proportional to the length of parallel overlaps and thus also lead to centering of off-centered kinetochores (**Fig. 1 A**).

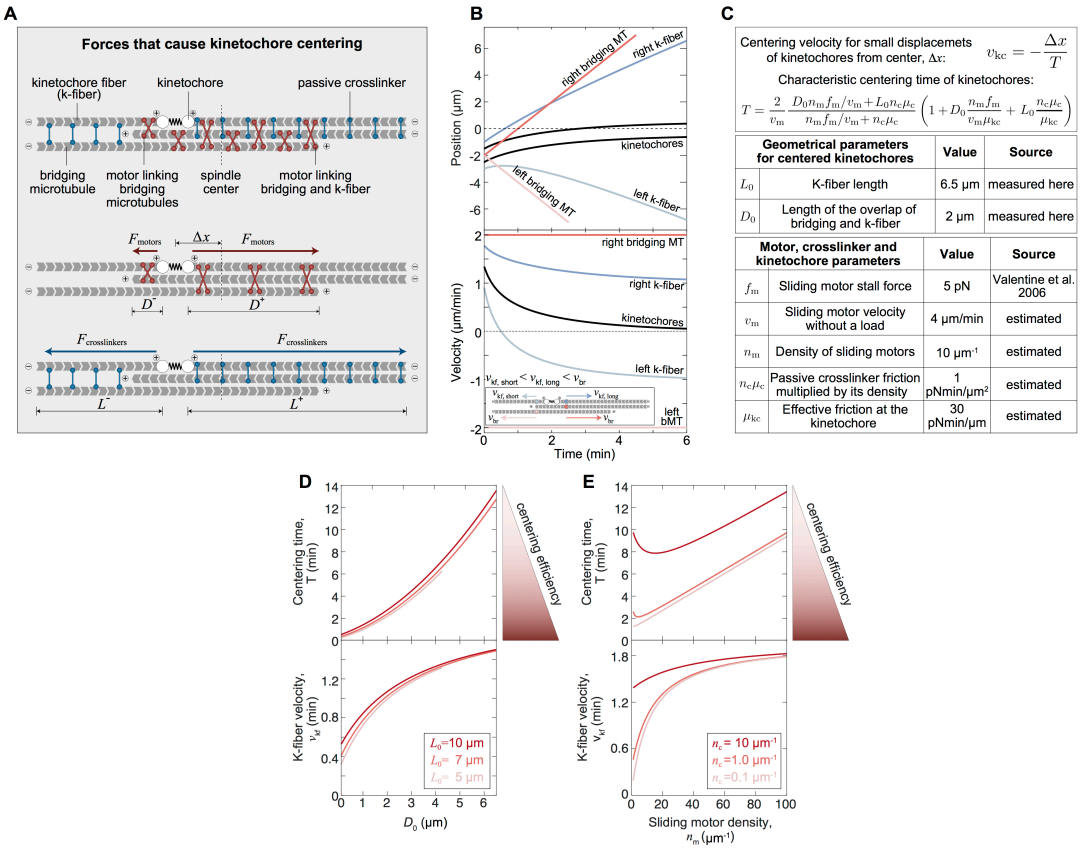

Figure 1. The theoretical model for chromosome centering. (**A**) Scheme of the model. Microtubules (grey lines) extend from the edges, where their minus ends are (minus sign), with plus ends (plus sign) towards kinetochores (white spheres) or towards microtubules from the opposite side. Motor proteins (red X-shapes) connect antiparallel microtubules and passive cross-linkers (blue I-shape) connect parallel microtubules. The lengths of kinetochore fibers are denoted by $\boldsymbol{L}^+$ and $\boldsymbol{L}^-$ and the lengths of the overlaps of bridging and kinetochore fibers are denoted by $\boldsymbol{D}^+$ and $\boldsymbol{D}^-$, where superscripts + and − denote the right and left sides, respectively. Kinetochores are connected by an elastic spring and displaced from the center by $\boldsymbol{\Delta x}$. The difference in forces when the number of motors or crosslinkers is different on the left and right sides is shown in the schemes below. (**B**) Solution of the model for initial displacement $\boldsymbol{\Delta x} = \ \boldsymbol{\mu}$**m.** Top: Positions of kinetochores (shades of blue), kinetochore fibers (black) and bridging microtubules (shades of red) are shown over time for parameters given in lower table in panel (C). Bottom: Velocities of kinetochores (shades of blue), kinetochore fibers (black) and bridging microtubules (shades of red) over time for the same parameters. A scheme is given showing the difference in velocities for fibers of different lengths. (**C**) Top: Formulas for the centering velocity and characteristic centering time of kinetochores for small displacements from center. Middle: Table with geometrical parameters for centered kinetochores, where $\boldsymbol{L}^+ = \boldsymbol{L}^- = \boldsymbol{L}$ and $\boldsymbol{D}^+ = \boldsymbol{D}^- = \boldsymbol{D}$. Bottom: Table with motor, cross-linker and kinetochore parameters of the model. One parameter value was taken from a previous study (Valentine et al., 2006). (**D**) Top: Characteristic centering time, obtained by formula from panel (C), when overlap and kinetochore fiber lengths are varied. Bottom: Velocities of kinetochore fibers for the same varied parameters. Right: Representation of how centering efficiency varies with characteristic centering time. (**E**) Top: Characteristic centering time, obtained by formula from panel (C), when motor and cross-linker densities

are varied. Bottom: Velocities of kinetochore fibers for the same varied parameters. Right: Representation of how centering efficiency varies with characteristic centering time.

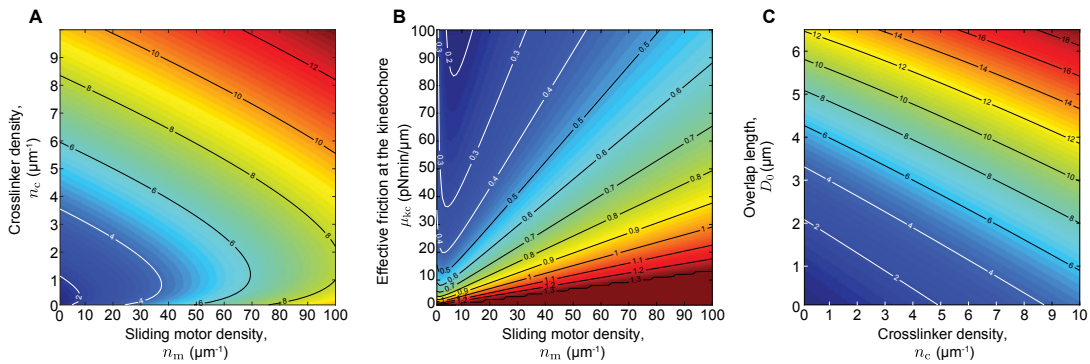

Figure S1. Heat plots for different parameters. Here the x and y axes show the variations of different parameters, while the characteristic centering time in minutes is shown through color intensity, ranging from blue to red. Black lines describe areas of parameter space with the same centering time. **(A)** The plot for the densities of cross-linkers and motors. **(B)** The plot for motor density and effective friction at the kinetochores. **(C)** The plot for cross-linker density and overlap length between k-fibers and bridging microtubules.

We solve the model for a pair of kinetochores that are initially displaced by 2 μm and find that they approach the center of the spindle in several minutes, for parameters typical for spindles in human cells (**Fig. 1 B,C**; **Methods**). While the bridging microtubules undergo poleward flux at a set velocity, k-fibers also flux but at a slower velocity (**Fig. 1 B**). When the kinetochores are displaced, the shorter k-fiber undergoes poleward flux at a slower velocity than the longer k-fiber (**Fig. 1 B**). The difference in poleward flux between two k-fibers, and thus also the centering velocity, decreases as the kinetochores approach the center (**Fig. 1 B**).

To understand the centering potential of the model, we solve the model in the vicinity of the center and find that the centering velocity of the kinetochores is the ratio of the displacement to the characteristic centering time, which describes centering efficiency (**Fig. 1 C; Methods**). A useful feature of our simple model is that it gives an explicit formula for the characteristic centering time (**Fig. 1 C**), which is not possible for complex models based on Monte Carlo simulations. As visible from the formula, the characteristic centering time depends on the geometry of the system, increasing with an increase in lengths of the parallel and antiparallel overlaps of bridging and k- fibers. It is also a function of densities of motor proteins and passive cross-linkers as well as their mechanical properties and those of kinetochores.

To explore what features of the system are crucial for efficient centering, we test the dependence of the characteristic centering time on various parameters, where shorter characteristic centering time means greater centering efficiency (**Fig. 1 D,E, Fig. S1**). We find that the length of antiparallel overlaps between bridging and k-

fibers is the key determinant of the centering efficiency (**Fig. 1 D**). It changes from 0.4 min for overlaps of zero length, which corresponds to the situation where bridging microtubules extending from one side of the spindle do not interact with the k-fiber on the opposite side, to 12.7 min for 6.5 µm long overlaps between a k-fiber and the bridging microtubules from the opposite side, which corresponds to overlaps that cover the entire spindle. Centering is better for short overlaps for two reasons: (i) the relative difference in the number of motors on either side is larger, resulting in a greater centering velocity and (ii) the difference between k-fiber velocities and bridging fiber velocities is larger (**Fig. 1 D**). Similarly, centering efficiency increases with decreasing spindle length, but the effect is smaller than for the overlap length (**Fig. 1 D**).

By varying the density of motor proteins we find a minimum of centering time, suggesting that around that point the centering mechanism behaves optimally (**Fig. 1 E**). Farther from the minimum, if the number of motors decreases, centering depends more on passive crosslinkers than on motors. Thus, centering becomes worse because the relative difference in passive crosslinkers on either side is smaller than the relative difference of motors, which is due to the geometry of the system. If the number of motors increases from the optimal one, the difference between k-fiber velocities and bridging fiber velocities decreases leading to worse centering. Similarly, by varying passive crosslinker density, we find that the centering time increases along with the passive crosslinker density (**Fig. 1 E**). Taken together, the mechanism of centering relies on the k-fibers undergoing flux at a smaller velocity than the bridging fiber. This allows for faster flux of the longer than the shorter k-fiber at displaced kinetochores, leading to fast movement of the kinetochores towards the spindle center.

Assay to follow the movement of individual microtubules within the spindle

To test the flux-driven centering model experimentally, it is important to measure the flux of different classes of microtubules (kinetochore and bridging). This has not been done until now in human spindles due to a lack of experimental methods for the analysis of the movement of individual microtubules. Thus we developed a speckle microscopy assay to study microtubules within spindles of the human non-cancer immortalized epithelial cell line hTERT-RPE1 (from here on referred to as RPE1), by using a very low concentration (1 nM) of SiR-tubulin (Lukinavicius et al., 2014). This resulted in a speckled signal of SiR-tubulin in the spindle (**Fig. 2 A**), which results from a few dye molecules within a resolution-limited region (Waterman-Storer and Salmon, 1998).

To distinguish between different classes of microtubules within the spindle, we divided the speckles into groups: (1) the speckles that originate close to a kinetochore, at the pole-facing side, were defined as those on a kinetochore microtubule (**Fig. 2 B**), (2) the speckles that pass the region between sister kinetochores, moving close to the kinetochores, were defined as those on a bridging microtubule (**Fig. 2 C**), (3) all other speckles in the spindle region between the

centrosomes, for which we cannot determine the type of microtubule they belong to, we refer to as "other" speckles (**Fig. 2 D**). This assay allowed us to study the movement of individual microtubules with respect to each other.

Bridging microtubules undergo poleward flux at a higher rate than kinetochore microtubules

We tracked each speckle (**Fig. 2 E**) and measured its distance to the centrosome over time (**Fig. 2 F-I).** The speckles on the k-fibers appeared at various distances in the range 4 - 9 µm from the pole, moved poleward and could be followed for about 1 minute before disappearing, presumably due to photobleaching (**Fig. 2 G**). The linear poleward velocity of speckles on kinetochore microtubules over the first 30 seconds of their movement was 1.18 ± 0.12 µm/min (n = 48 speckles from 22 cells) (**Fig. 2 J; Fig. S2 A; Table 1**). This velocity is similar to the rate of poleward flux previously measured by tubulin photoactivation on kinetochore fibers in RPE1 cells expressing photoactivatable-GFP-α-tubulin, 1.09 ± 0.11 µm/min (Dudka et al., 2018). This validates our identification of speckles on k-fibers.

In the flux-driven centering model, kinetochores become centered only if the poleward flux of the bridging microtubules is faster than the flux of k-fibers. In our experiments, speckles on the bridging microtubules appeared in the range 5 - 10 µm from the pole, moved poleward, and could be followed typically over 1 minute (**Fig. 2 H**). Remarkably, the speckles on bridging microtubules moved poleward at a velocity of 2.09 ± 0.20 µm/min (n = 43 speckles from 24 cells) (**Fig. 2 J; Fig. S2 A; Table 1**), which is significantly faster than for the speckles on kinetochore microtubules ($p = 0.0002$).

The mechanism of kinetochore centering in the model relies on faster flux of the longer than of the shorter k-fiber at displaced kinetochores, which leads to the movement of the kinetochores towards the spindle center. To explore whether such a difference in the flux of short and long k-fibers exist in spindles, we divided the speckles on k-fibers into 3 groups: those on short, medium, and long k-fibers (starting distance from the pole at <0.4, between 0.4 and 0.6, and >0.6 of the spindle length, respectively). Strikingly, the speckle poleward velocity increased with an increasing k-fiber length (**Fig. 2 K**). Short k-fibers had a flux of 0.85 ± 0.15 µm/min (n = 23 speckles from 25 cells), whereas the flux of long k-fibers was significantly faster, 1.53 ± 0.26 µm/min (n = 10 speckles from 25 cells, $p = 0.02$). In addition, flux velocities of all speckles together were higher for those that started at a larger distance from the pole (**Fig. 2 L**). Thus, the spindles exhibit the key features of the flux-driven centering model, where different subsets of fibers show different flux velocities.

Because our experiments provide the first measurement of poleward flux of bridging microtubules in human spindles, we decided to validate our method of identification of speckles in the bridging fiber. We used PRC1 siRNA, which is known to specifically reduce the number of bridging microtubule to ~50% of the original number (Jagrić et al., 2021; Polak et al., 2017). In cells treated with PRC1 siRNA, we observed 10 speckles on bridging microtubules in 11 cells, which is

roughly a 2-fold reduction in comparison with untreated cells, 43 speckles in 27 cells, providing support for our method (**Fig. S2 B**).

Given that the spindle length is constant during metaphase, the antiparallel bridging microtubules slide apart at twice the rate of their poleward flux, 4.2 ± 0.2 µm/min. This rate is comparable to the sliding rate of bridging microtubules in early anaphase measured by photoactivation, which is roughly 4.5 µm/min (Vukusic et al., 2019), suggesting that the bridging microtubule sliding is driven by a similar mechanism in metaphase and early anaphase. However, in contrast to early anaphase where kinetochore fibers and bridging fibers slide together at a similar rate (Vukusic et al., 2017), in metaphase kinetochore fibers move slower than bridging fibers. This difference is most likely due to the chromatin link between sister kinetochore fibers during metaphase. Thus, kinetochore fibers slip during their poleward movement with respect to bridging fibers in metaphase, but not in anaphase.

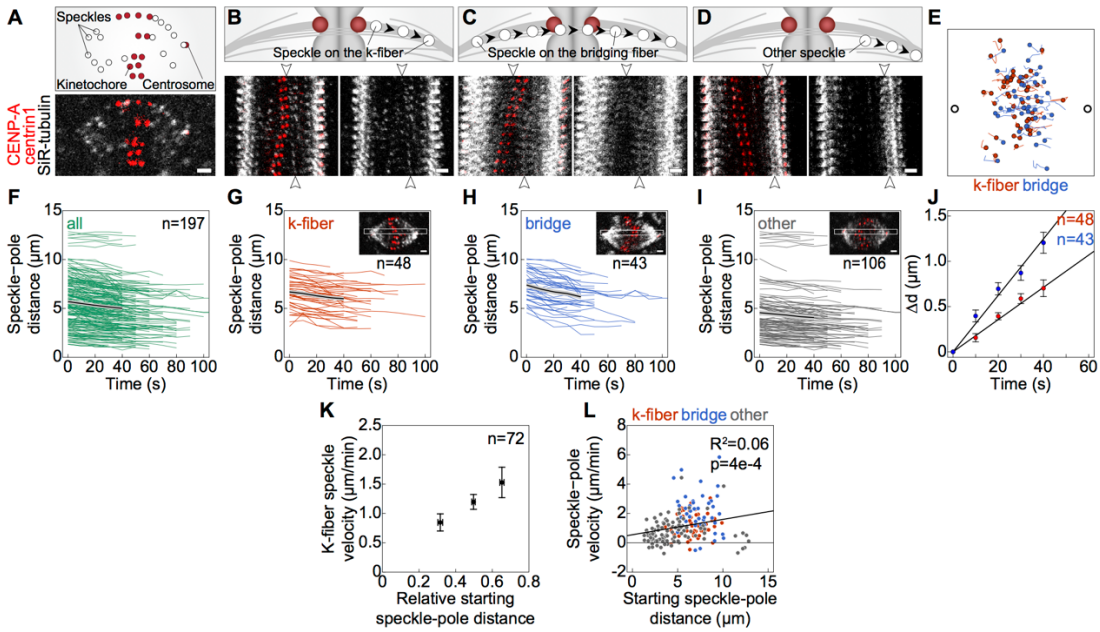

Figure 2. (**A**) Spindle in a RPE1 cell stably expressing CENP-A-GFP and centrin1-GFP (red) stained with 1 nM SiR-tubulin dye which appears as distinct speckles marking individual microtubules (grey). (**B**) Scheme of the speckle originating at kinetochore defined as the one marking the k-fiber microtubule (top). Montage over time demonstrating the movement of speckle belonging to the k-fiber microtubule (bottom). Merge (left); tubulin channel only (right). Arrowheads mark starting and ending positions of the tracked speckle. (**C**) Scheme of the speckle passing the region between sister kinetochores, moving close to the kinetochores, defined as the one marking microtubule within the bridging fiber (top). Montage over time demonstrating the movement of speckle belonging to the bridging fiber microtubule. Legend as in B. (**D**) Scheme of other speckles for which it could not be determined the type of microtubule they belong to (top). Montage over time demonstrating the movement of this group of speckles. Legend as in B. (**E**) Tracks of speckles belonging to k-fibers (red) and bridging fibers (blue). (**F-I**) Distance of all, k-fiber, bridging fiber and other speckles from the pole over time in untreated cells. Colored lines show individual speckles. Black line; mean.

Grey area; s.e.m. Rectangles on the spindles inside graphs mark the regions for which montages in B-D are generated. (**J**) Change in speckle-pole distance over time. (**K**) Poleward velocity of k-fiber depending on its relative starting speckle-pole distance. (**L**) Poleward velocity of k-fiber, bridging and other speckles versus the distance of their starting position from the pole. Black line shows linear regression. Error bars; s.e.m. n; number of measurements. Scale bars; 2 µm. Statistical analysis, t-test. R^2, coefficient of determination. p-value legend: < 0.0001 (****), 0.0001 to 0.001 (***), 0.001 to 0.01 (**), 0.01 to 0.05 (*), ≥ 0.05 (ns).

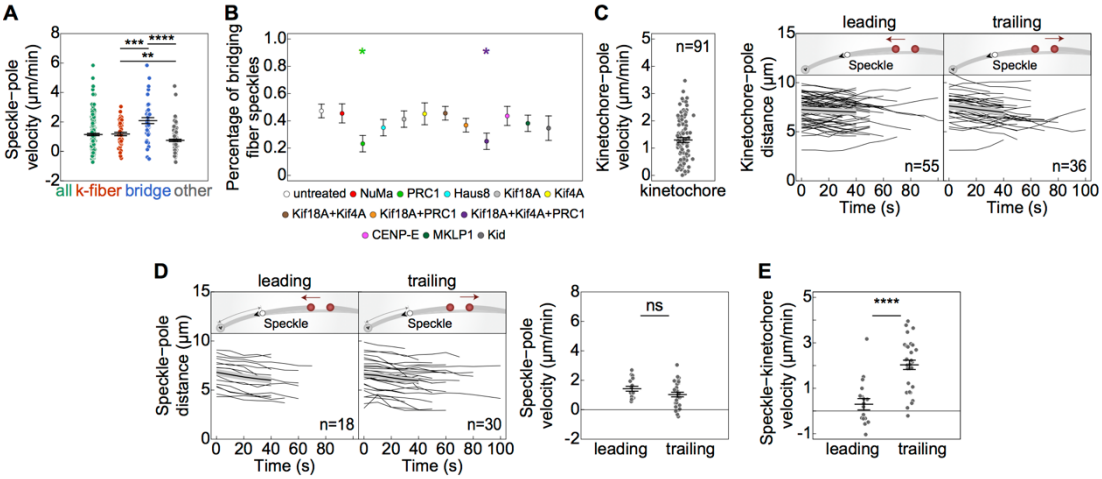

Figure S2. (**A**) Poleward velocity of the speckles shown in Fig. 2 F-I. Each dot corresponds to individual speckle. (**B**) Ratio of tracked speckles within bridging fibers and bridging and k-fibers color-coded for siRNA treatment. (**C**) Graph of kinetochore poleward velocity (left). Each dot corresponds to individual kinetochore pair. Distance between leading kinetochore (middle) and trailing (right) kinetochore from the pole. (**D**) Distance between speckles on the leading (left) and trailing (middle) kinetochore microtubules from the pole. Poleward velocity of speckles on leading and trailing kinetochore microtubules (right). (**E**) Velocity of speckles on leading and trailing kinetochore microtubules moving away from the corresponding kinetochore. Error bars; s.e.m. n; number of measurements.

Leading kinetochore microtubules are largely in a pausing state, while trailing microtubules polymerize

Throughout metaphase, kinetochores oscillate around the equatorial plane of the spindle. During the periods of time when a pair of sister kinetochores moves at a roughly constant velocity towards one pole, this velocity was 1.4 ± 0.1 µm/min (n = 91 kinetochore pairs from 27 cells) (**Fig. S2 C**). The speckles on the leading kinetochore microtubules, which are linked to the pole towards which the kinetochores are traveling, moved poleward at a velocity of 1.4 ± 0.2 µm/min (n = 18 speckles from 27 cells) (**Fig. S2 D**). However, this value is likely overestimated because only those speckles that move poleward faster than the kinetochores and thus are not "chewed up" by the kinetochore can be tracked. These speckles on the leading k-fiber moved away from kinetochore at a velocity of 0.3 ± 0.2 µm/min (n =18

speckles from 27 cells), implying that kinetochore microtubules at the leading side are largely in a pausing state (**Fig. S2 E**). Even though we cannot exclude that in some cases of oscillations the leading k-fiber depolymerizes, this result indicates that kinetochores can move poleward while their leading k-fiber microtubules are in a pausing state or polymerize slowly.

Speckles on the trailing kinetochore microtubules moved poleward at velocity of 1.0 ± 0.2 µm/min (n =30 speckles from 27 cells), which was not different from the leading side (p=0.08) (**Fig. S2 D**). These speckles moved away from the kinetochore at a velocity of 2.0 ± 0.2 µm/min (n =30 speckles from 27 cells), which corresponds to the polymerization rate of kinetochore microtubules at the trailing side (**Fig. S2 E**). Taken together, these result show that kinetochore microtubules are mainly in a polymerizing or a pausing state.

Sliding forces from the bridging fiber are transmitted onto the associated k-fiber

To explore how the sliding of the bridging microtubules and the poleward flux of k-fibers are related to each other and to kinetochore alignment, we performed a set of perturbations in which we depleted candidate microtubule-associated proteins by siRNA. First, we depleted non-motor proteins that are important for k-fiber and bridging fiber integrity and their crosslinking. Then we depleted motor proteins that localize to the bridging fiber and regulate microtubule dynamics and/or generate microtubule sliding.

We started with NuMa, a protein that is required for local load-bearing in the spindle (Elting et al., 2017) and for synchronous microtubule flux across the spindle (Steblyanko et al., 2020). Thus we hypothesized that NuMa may be one of the main crosslinkers of kinetochore and bridging microtubules extending from the same spindle half, i.e., aligned in a parallel orientation. To explore this hypothesis, we depleted NuMa by siRNA (**Fig. S3**) and found that the flux velocity of bridging fibers did not change, whereas the flux velocity of kinetochore microtubules decreased by ~38% (from 1.18 ± 0.12 in untreated cells to 0.72 ± 0.17 after NuMa depletion, **Fig. 3 A,B; Fig. S4 A; Table 1**). These results support the model in which the sliding apart of bridging microtubules is transmitted through NuMa to kinetochore microtubules, which flux slower when this connection is weakened.

To perturb specifically bridging fibers, we depleted PRC1 (**Fig. S3**), which results in ~50% decrease of the number of microtubules in the bridging fiber without affecting the length of their antiparallel overlaps (Jagrić et al., 2021). We found that depletion of PRC1 did not change the flux velocity of bridging or kinetochore microtubules (**Fig. 3 B; Fig. S4 B; Table 1**), in agreement with a previous result based on tubulin photoactivation (Steblyanko et al., 2020). This result suggests that the bridging microtubules that remain after PRC1 depletion are sufficient to generate sliding.

The augmin complex promotes nucleation of new microtubules at the wall of existing microtubules (David et al., 2019; Goshima et al., 2008; Kamasaki et al.,

2013). Depletion of the Haus8 subunit of the augmin complex results in ~50% decrease of the number of microtubules in the bridging fiber and ~30% in the k-fiber, together with an elongation of the PRC1-labeled antiparallel overlaps of bridging microtubules (Manenica et al., 2020). When we depleted Haus8, we measured ~52% slower flux of the bridging microtubules, while the flux of kinetochore microtubules decreased ~18% (**Fig. 3 B; Fig. S4 C; Table 1**). Given that after Haus8 depletion most of the microtubules are nucleated at the spindle pole, we speculate that the mechanisms driving microtubules depolymerization at the pole limit their velocity of flux.

To explore how k-fibers affect the sliding of bridging microtubules, we depleted Ndc80, the main coupler of kinetochores to microtubule ends (Cheeseman et al., 2006; Cheeseman and Desai, 2008). Reduction of k-fibers was confirmed by the observation that speckles at the pole-facing side of the kinetochore were not found (n=8 cells). We found that the speckles on bridging microtubules fluxed at a similar velocity as in untreated cells (**Fig. 3 B; Fig. S4 D; Table 1**), suggesting that k-fibers do not act as a brake for the sliding of bridging microtubules.

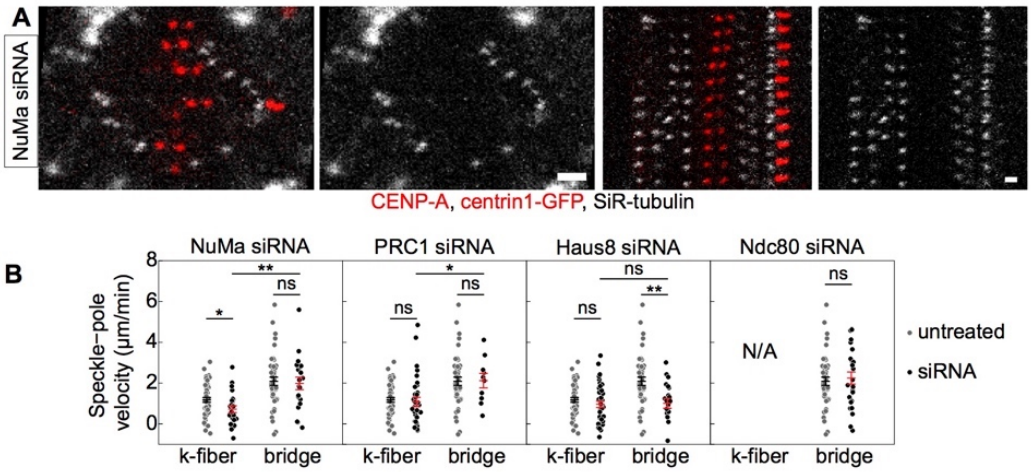

Figure 3. (**A**) Spindle in a RPE1 cell stably expressing CENP-A-GFP and centrin1-GFP (red) treated depleted for NuMa and stained with 1 nM SiR-tubulin dye (left). Montage over time for speckle movement in spindle on left (right). Merge (left); tubulin channel only (right).
(**B**) Speckles after depletion of NuMa, PRC1, Haus8 and Ndc80 (left to right). Graphs show poleward velocity of the speckles in siRNA-treated (black) and control (grey) cells. Scale bars; 2 µm. Statistical analysis, t-test. p-value legend as in Fig. 2.

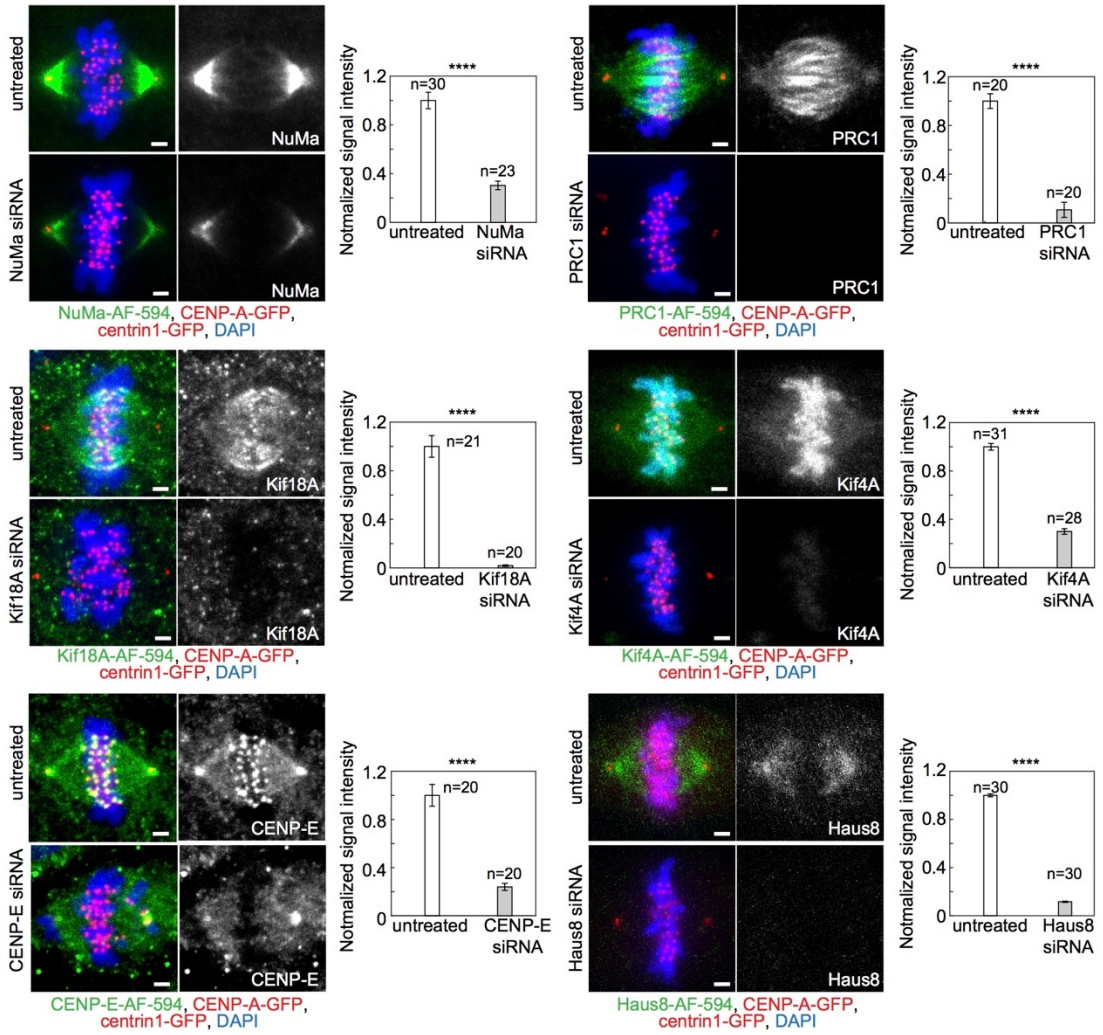

Figure S3. Fixed spindles in a RPE1 cell stably expressing CENP-A-GFP and centrin1-GFP (red) in cells immunostained for NuMa (AF-594, green) (upper left), PRC1 (AF-594, green) (upper right), Kif18A (AF-594, green) (middle left), Kif4A (AF-594, green) (middle right), CENP-E (AF-594, green) (bottom left) and Haus8 (AF-594, green) (bottom right) in untreated (upper rows) and corresponding siRNA-treated cells (bottom rows), with DNA stained with DAPI (blue). Left; merge; protein of interest; right (grey). Graphs showing intensities of indicated proteins in untreated (white bars) and siRNA treated (grey bars) cells are given on the right. All values are normalized on the mean intensity value of untreated cells for each protein. All treatments include at least two independent experiments. n; number of cells. Scale bars; 2 µm. All images are maximum intensity projections of five z-planes smoothed with 0.5-pixel-sigma Gaussian blur. Statistical analysis, t-test. p-value legend as in Fig. 2.

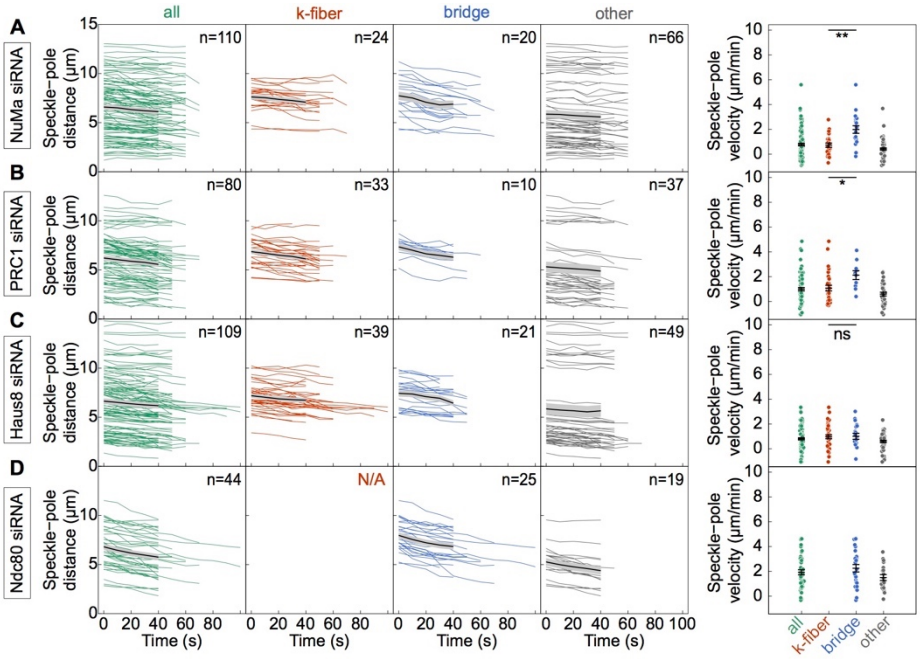

Figure S4. Speckles after depletion of NuMa (**A**), PRC1 (**B**), Haus8 (**C**) and Ndc80 (**D**). Graphs from left to right show: distance between speckles and the spindle pole over time for all speckles, speckles on kinetochore microtubules, speckles on bridging microtubules, other speckles. Colored lines show individual speckles. Black line; mean. Grey area; s.e.m. Poleward velocity of the speckles is shown at the right. Error bars; s.e.m. All treatments include at least three independent experiments. n; number of measurements. Statistical analysis, t-test. p-value legend as in Fig. 2.

Motor proteins that localize within the bridging fiber modulate the flux velocity of bridging and kinetochore microtubules

Next, we depleted motor proteins that localize to the bridging fiber and regulate microtubule dynamics and/or generate microtubule sliding (**Fig. 4**). Kinesin-8 proteins are major regulators of chromosome alignment in various organisms from yeast to humans (Garcia et al., 2002; Stumpff et al., 2008; Wargacki et al., 2010). The human kinesin-8 Kif18A accumulates to the plus end of kinetochore microtubules, where it suppresses microtubules dynamics (Du et al., 2010; Stumpff et al., 2012). Kif18A also localizes within bridging fibers and regulates the length of their antiparallel overlap regions (Jagrić et al., 2021). When we depleted Kif18A (**Fig. S3**), we found that the flux velocity of bridging fibers did not change, whereas the flux velocity of kinetochore microtubules increased by ~55% (from 1.18 ± 0.12 in untreated cells to 1.83 ± 0.32 after Kif18A depletion, **Fig. 4 A; Fig. S5 A; Table 1**).

Kinesin-4 proteins are chromokinesins that regulate microtubule dynamics (Bieling et al., 2010b; Bringmann et al., 2004; Stumpff et al., 2012; Wandke et al., 2012) and generate polar ejection forces (Bieling et al., 2010a; Brouhard and Hunt, 2005). Kif4A, a human kinesin-4, localizes during metaphase to bridging fibers in

addition to its prominent localization on chromosome arms, and regulates the length of the antiparallel overlaps of bridging microtubules (Jagrić et al., 2021). After depletion of Kif4A (**Fig. S3**), we measured that the flux velocity of bridging microtubules did not change, whereas the flux velocity of kinetochore microtubules increased by ~49% (from 1.18 ± 0.12 in untreated cells to 1.76 ± 0.33 after Kif4A depletion, **Fig. 4 A; Fig. S5 B; Table 1**), similar to Kif18A depletion. In contrast, depletion of the chromokinesin Kid (Levesque and Compton, 2001; Wandke et al., 2012) did not affect flux velocities (**Fig. 4 A**).

Next, we explored the role of CENP-E in the flux of bridging and kinetochore microtubules. A role of this protein in flux has been demonstrated during prometaphase (Steblyanko et al., 2020). Depletion of CENP-E (**Fig. S3**) resulted in a significant reduction of flux velocity both for bridging and kinetochore microtubules in metaphase (**Fig. 4 A; Fig. S5; Table 1**). These two velocities were similar in CENP-E depleted cells. Given that CENP-E localizes to bridging fibers in metaphase (Steblyanko et al., 2020), we propose that CENP-E within the bridge contributes to the sliding of bridging microtubules during metaphase. Unlike CENP-E, depletion of the kinesin-6 MKLP1 (Gruneberg et al., 2006; Mishima et al., 2002) did not change flux velocities (**Fig. 4 A; Fig. S5**).

To decouple the mechanism of kinetochore centering by poleward flux from the effects of Kif18A on the k-fiber plus ends, we combined Kif18A depletion with depletions of other proteins. Double depletion of Kif18A and Kif4A, double depletion of Kif18A and PRC1, and triple depletion of Kif18A, Kif4A, and PRC1 resulted in an increase in the flux velocity of kinetochore microtubules, with no effect on the bridging fiber flux (**Fig. 4 B,C; Fig. S5; Table 1**). As in untreated cells, the flux velocity in these treatments increased with an increasing k-fiber length (**Fig. 4 D**).

Taken together, in Kif4A depletion and all depletions that include Kif18A kinetochore microtubules slide at a velocity that is indistinguishable from the sliding velocity of bridging microtubules, suggesting a stronger coupling between bridging and kinetochore microtubules. We hypothesized that this may be due to longer overlaps of bridging microtubules, which imply longer overlaps between a k-fiber and its bridging fiber. In agreement with previous results on HeLa cells (Jagrić et al., 2021), Kif4A depletion and Kif18A depletion in RPE1 cells resulted in an increased length of PRC1-labeled streaks marking antiparallel overlaps of bridging microtubules (**Fig. 4 E,F**; **Table 1**). Double depletion of Kif18A and Kif4A resulted in a similar increase, close to single Kif18A depletion (**Fig. 4 F**; **Table 1**). Thus, similar velocities of bridging and k-fiber flux are correlated with an increased overlap length, supporting the role of antiparallel overlaps in the coupling between bridging and k-fibers.

Both single Kif4A and Kif18A depletions led to an increased spindle length, similar to the results on HeLa cells (Jagrić et al., 2021), and the double depletion resulted in the largest increase in spindle length (**Table 1**). It is reasonable to assume that longer spindles have longer k-fibers and thus the overlaps between a k-fiber and the bridging microtubules extending from the same spindle half are also longer, which may further increase the mechanical coupling between bridging and k-fibers.

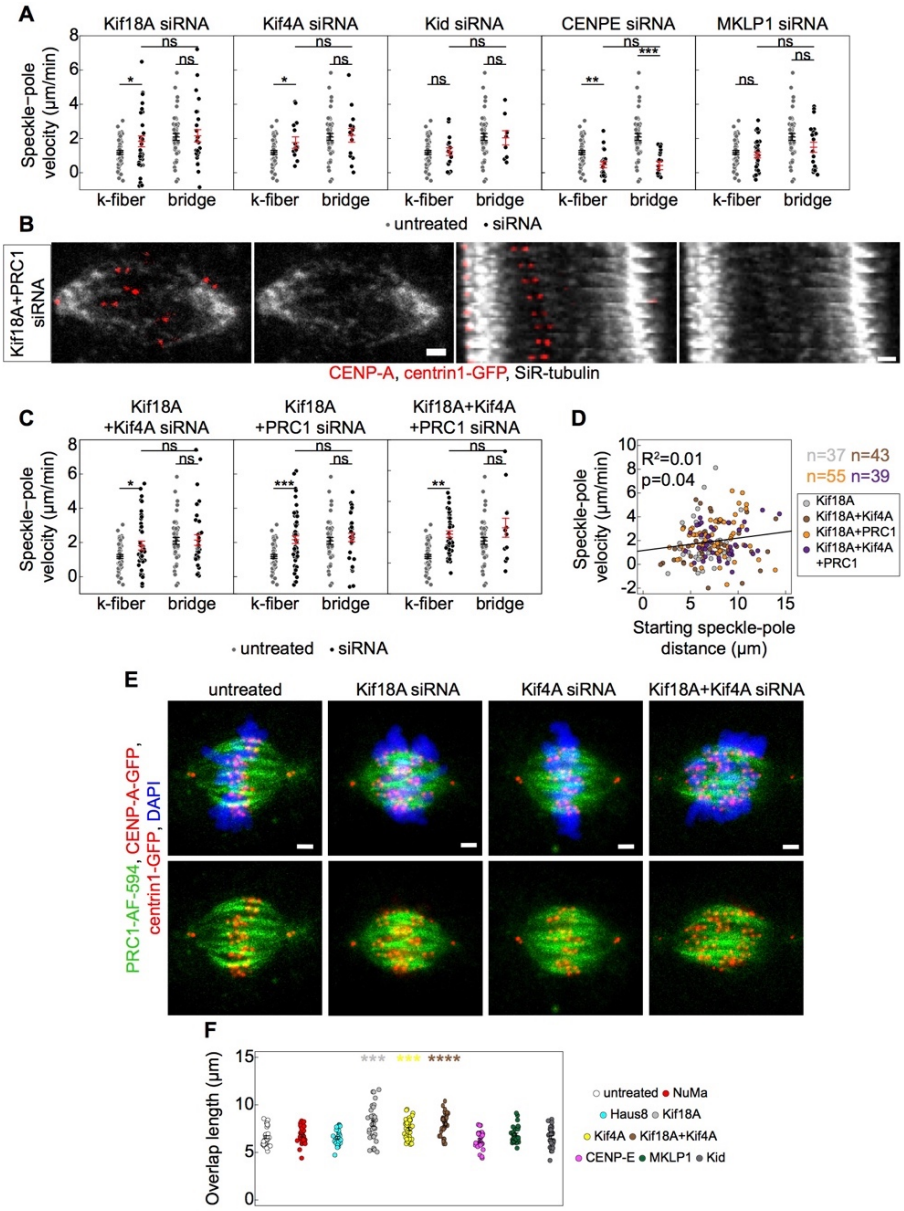

Figure 4. (**A**) Speckles after depletion of Kif18A, Kif4A, Kid, CENP-E and MKLP1 (left to right). Graphs show poleward velocity of the speckles in siRNA-treated (black) and control (grey) cells. (**B**) Spindle in a RPE1 cell stably expressing CENP-A-GFP and centrin1-GFP (red) depleted for Kif18A and PRC1, stained with 1 nM SiR-tubulin dye (left). Montage over time for speckle movement in spindle on the left (right). Merge (left); tubulin channel only (right). (**C**) Speckles after depletion of Kif18A and Kif4A, Kif18A and PRC1, and Kif18A, Kif4A and PRC1 (left to right). Graphs show poleward velocity of the speckles in siRNA-treated (black) and control (grey) cells. (**D**) Poleward velocity of k-fiber versus the distance of their starting position from the pole. Black line shows linear regression. (**E**) Fixed spindles in RPE1 cells stably expressing CENP-A-GFP and centrin1-GFP (red) in untreated (first column), Kif18A siRNA (second column), Kif4A siRNA (third column), and Kif18A and Kif4A siRNA treated cells (fourth column), immunostained for endogenous PRC1 (AF-594, green) and stained with DAPI (blue). Upper row; merge, bottom row; GFP and AF-594. All images are maximum intensity projections of five z-planes smoothed with 0.5-pixel-sigma

Gaussian blur. (**F**) Length of PRC1-labeled overlaps. All treatments include at least three independent experiments. Error bars; s.e.m. n; number of measurements. Scale bars; 2 µm. Statistical analysis, t-test. R^2, coefficient of determination. p-value legend as in Fig. 2.

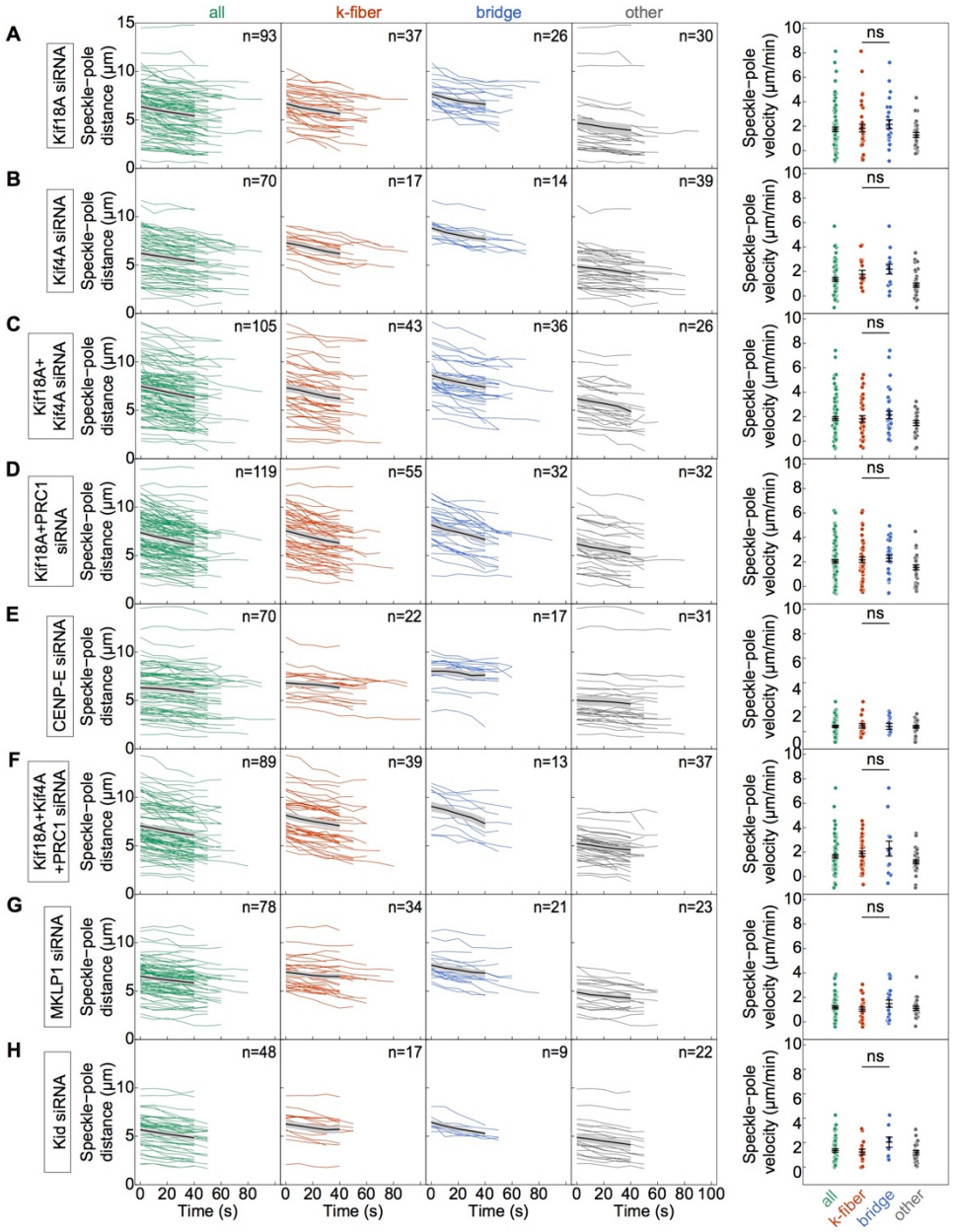

Figure S5. Speckles after depletion of Kif18A (**A**), Kif4A (**B**), Kif18A and Kif4A (**C**), Kif18A and PRC1 (**D**), CENP-E (**E**), Kif18A, Kif4A and PRC1 (**F**), MKLP1 (**G**) and Kid (**H**). Graphs from left to right show: distance between speckles and the spindle pole over time for all speckles, speckles on kinetochore microtubules, speckles on bridging microtubules, other speckles. Colored lines show individual speckles. Black line; mean. Grey area; s.e.m. Poleward velocity of the speckles is shown at the right. Error bars; s.e.m. All treatments include at least three independent experiments. n; number of measurements. Statistical analysis, t-test. p-value legend as in Fig. 2.

Forces within the bridging fiber have a centering effect on the kinetochores

To explore the role of the selected proteins in kinetochore alignment in treatments which do not perturb biorientation, we quantified the alignment efficiency by measuring the distances of sister kinetochore midpoints from the equatorial plane, d_{EQ} (**Fig. 5 A, B**). Among the single protein depletions, only Kif18A, as well as Ndc80 which does not have bioriented kinetochores, resulted in a significantly larger d_{EQ} implying kinetochore misalignment (**Fig 5 B; Table 1**). This is in agreement with the known major role of Kif18A in the positioning of bioriented kinetochore (Mayr et al., 2007; Stumpff et al., 2008).

To uncouple the role of forces generated within the bridging fiber from the function of Kif18A in kinetochore alignment, we used a double depletion of Kif18A and Kif4A, double depletion of Kif18A and PRC1, and a triple depletion of Kif18A, Kif4A, and PRC1. Strikingly, the combined depletions showed remarkable kinetochore misalignment, reflected in a significantly increased d_{EQ} with respect to Kif18A depletion (**Fig. 5 B,** see also **Fig. 4 E; Table 1**). Thus, in the absence of Kif18A, Kif4A and PRC1 promotes kinetochore alignment, where Kif4A possibly acts through its activity on chromosome arms in generating polar ejection forces and both proteins via their role in regulating bridging microtubules.

The four depletion conditions with the strongest kinetochore misalignment, Kif18A alone and in combination with Kif4A and/or PRC1, had larger spindle lengths than untreated cells and most other conditions (**Fig. 5 C,D**), and larger PRC1-labeled overlap length (**Fig. 5 E**). Importantly, these four conditions had a significantly faster k-fiber flux than most other cases, whereas the bridging fiber flux was not different than in untreated cells (**Fig. 5 F,G**). Thus, we conclude that the relative sliding of the k-fibers with respect to the bridging fiber is important for kinetochore alignment, in agreement with the flux-driven centering model.

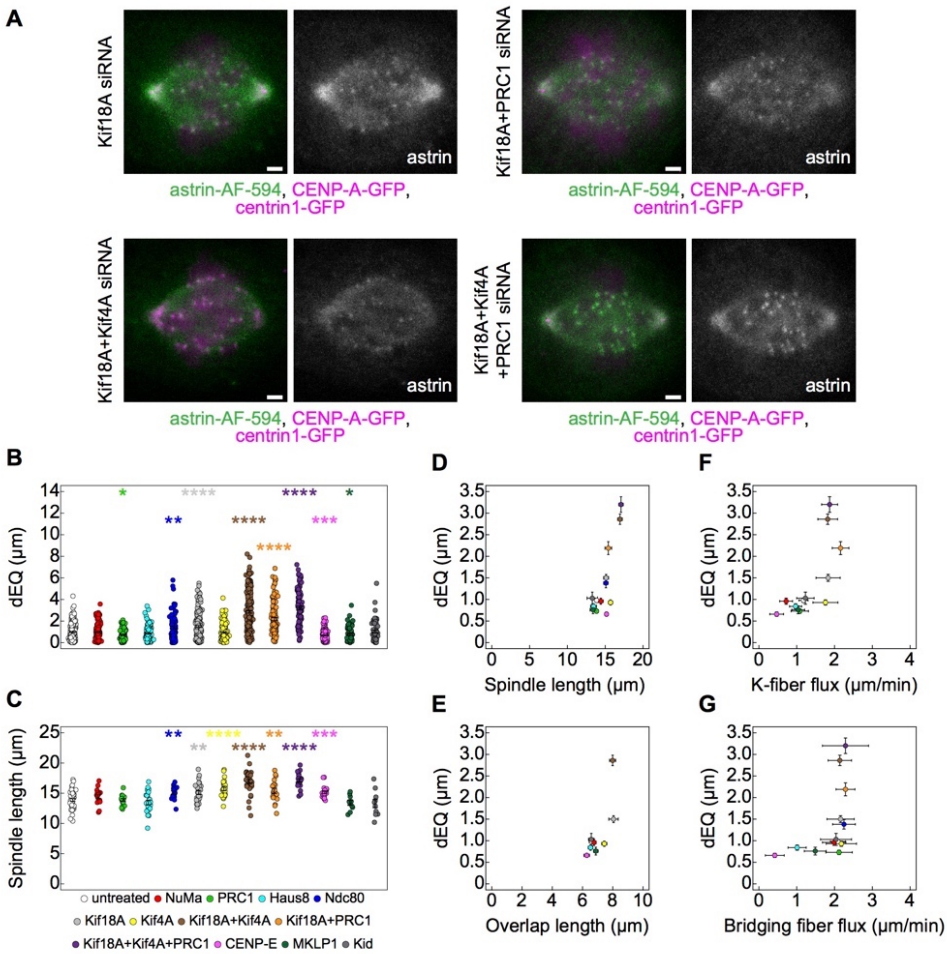

Figure 5. (**A**) Fixed spindles in RPE1 cells stably expressing CENP-A-GFP and centrin1-GFP (magenta), immunostained for astrin (AF-594, green) and treated with Kif18A (top left), Kif18A and Kif4A (bottom left), Kif18A and PRC1 (top right) and Kif18A, Kif4A and PRC1 (bottom right) siRNA. Left; merge; astrin; right (grey). (**B**) Distance of sister kinetochore midpoints from the equatorial plate (d_{EQ}) for untreated and siRNA treated cells. Treatments are color-coded according to the legend (bottom left). (**C**) Spindle lengths for cells as in B. (**D**) d_{EQ} versus spindle length for cells as in B. (**E**) d_{EQ} versus PRC1-labeled overlap length for cells as in B. (**F**) d_{EQ} versus k-fiber speckle poleward velocity for cells as in B. (**G**) d_{EQ} versus bridge speckle poleward velocity for cells as in B. Asterisks denote significance with respect to untreated cells. Statistical analysis; t-test. p-value legend as in Fig. 2.

Table 1. Measurements of flux, spindle and kinetochore parameters.

Values are given as mean ± sem. The numbers in brackets denote the number of measurements (number of speckles for flux measurements or number of kinetochore pairs; for spindle length this number is not given because it is equal to the number of cells), number of cells, and p-value from a t-test for comparison with untreated cells. *n.a.*, not applicable; *n.d.*, not determined.

	Flux, all (µm/min)	Flux, k-fiber (µm/min)	Flux, bridge (µm/min)	Flux, other (µm/min)	Spindle length (µm)	Overlap length (µm)	Inter-kinetochore distance (µm)	Kinetochore distance to equatorial plane (µm)
Untreated	1.14 ± 0.08 (197, 27, n.a.)	1.18 ± 0.12 (48, 27, n.a.)	2.09 ± 0.20 (43, 27, n.a.)	0.75 ± 0.08 (106, 27, n.a.)	13.87 ± 0.23 (44, n.a.)	6.6 ± 0.2 (33, 11, n.a.)	0.94 ± 0.01 (258, 44, n.a.)	0.98 ± 0.05 (258, 44, n.a.)
NuMa	0.77 ± 0.10 (110, 13, 0.005)	0.72 ± 0.17 (24, 13, 0.03)	1.99 ± 0.31 (20, 13, 0.9)	0.41 ± 0.09 (66, 13, 0.006)	14.42 ± 0.32 (17, 0.18)	6.8 ± 0.1 (33, 10, 0.45)	0.95 ± 0.02 (130, 17, 0.7)	0.96 ± 0.07 (130, 17, 0.7)
PRC1	0.99 ± 0.13 (80, 11, 0.3)	1.08 ± 0.23 (33, 11, 0.6)	2.12 ± 0.35 (10, 11, 0.9)	0.59 ± 0.15 (37, 11, 0.3)	13.86 ± 0.24 (15, 0.97)	n.a.	0.87 ± 0.01 (93, 15, 2e-5)	0.73 ± 0.05 (93, 15, 0.01)
Haus8	0.81 ± 0.09 (109, 14, 0.009)	0.97 ± 0.16 (39, 14, 0.2)	1.01 ± 0.24 (21, 14, 0.001)	0.59 ± 0.09 (49, 14, 0.2)	13.46 ± 0.38 (23, 0.36)	6.5 ± 0.1 (30, 13, 0.7)	0.81 ± 0.01 (137, 23, 2.2e-16)	0.84 ± 0.06 (137, 23, 0.09)
Ndc80	1.92 ± 0.20 (44, 8, 1e-04)	n.a.	2.25 ± 0.30 (25, 8, 0.6)	1.50 ± 0.24 (19, 8, 6e-04)	15.09 ± 0.29 (15, 0.002)	n.d.	0.81 ± 0.01 (105, 15, 2e-12)	1.38 ± 0.11 (105, 15, 0.003)
Kif18A	1.75 ± 0.18 (93, 21, 4e-04)	1.83 ± 0.32 (37, 21, 0.04)	2.16 ± 0.36 (26, 21, 0.8)	1.28 ± 0.20 (30, 21, 0.004)	15.12 ± 0.33 (25, 0.003)	8.1 ± 0.3 (35, 14, 1e-04)	0.90 ± 0.01 (198, 28, 0.01)	1.50 ± 0.08 (198, 28, 9e-6)
Kif4A	1.35 ± 0.16 (70, 10, 0.2)	1.76 ± 0.33 (17, 10, 0.04)	2.18 ± 0.40 (14, 10, 0.8)	0.87 ± 0.16 (39, 10, 0.4)	15.70 ± 0.28 (25, 7e-06)	7.4 ± 0.2 (39, 10, 6e-04)	1.06 ± 0.02 (165, 25, 2e-8)	0.93 ± 0.06 (165, 25, 0.4)
Kif18A+ Kif4A	1.84 ± 0.16 (105, 23, 1e-04)	1.82 ± 0.26 (43, 23, 0.02)	2.14 ± 0.31 (36, 23, 0.8)	1.47 ± 0.20 (26, 23, 2e-04)	16.96 ± 0.31 (37, 1e-11)	8 ± 0.2 (35, 13, 1e-04)	0.83 ± 0.01 (235, 37, 2e-13)	2.86 ± 0.12 (235, 37, 2e-16)
Kif18A + PRC1	2.03 ± 0.14 (119, 16, 1e-04)	2.16 ± 0.22 (55, 16, 3e-04)	2.29 ± 0.26 (32, 16, 0.5)	1.54 ± 0.20 (32, 16, 1e-04)	15.41 ± 0.44 (18, 0.005)	n.a.	0.80 ± 0.01 (116, 18, 1e-14)	2.19 ± 0.15 (116, 18, 8e-15)
Kif18A + Kif4A + PRC1	1.65 ± 0.15 (89, 17, 0.001)	1.87 ± 0.21 (39, 17, 0.003)	2.29 ± 0.61 (13, 17, 0.6)	1.20 ± 0.15 (37, 17, 0.006)	17.09 ± 0.29 (20, 4e-11)	n.a.	0.80 ± 0.01 (91, 20, 3e-14)	3.20 ± 0.18 (91, 20, 2e-16)

CENP-E	0.42 ± 0.09 (70, 9, 1e-04)	0.47 ± 0.18 (22, 9, 0.001)	0.42 ± 0.25 (17, 9, 1e-04)	0.39 ± 0.11 (31, 9, 0.02)	15.17 ± 0.23 (20, 2e-04)	6.3 ± 0.2 (28, 11, 0.17)	0.94 ± 0.02 (122, 25, 0.9)	0.66 ± 0.05 (122, 25, 0.0001)
MKLP1	1.18 ± 0.12 (78, 13, 0.8)	1.04 ± 0.17 (34, 13, 0.5)	1.49 ± 0.29 (21, 13, 0.09)	1.10 ± 0.17 (23, 13, 0.06)	13.39 ± 0.39 (10, 0.3)	6.9 ± 0.1 (32, 14, 0.2)	0.90 ± 0 0.02 (57, 10, 0.02)	0.76 ± 0.09 (57, 10, 0.02)
Kid	1.35 ± 0.14 (48, 7, 0.2)	1.23 ± 0.23 (17, 7, 0.8)	2.04 ± 0.41 (9, 9, 0.9)	1.16 ± 0.18 (22, 7, 0.03)	13.29 ± 0.69 (10, 0.4)	6.6 ± 0.2 (33, 12, 0.9)	0.93 ± 0.02 (57, 10, 0.5)	1.03 ± 0.14 (57, 10, 0.5)

DISCUSSION

Based on our model and the results from speckle microscopy that allowed us to measure the relative movements of kinetochore and bridging microtubules in normal and perturbed spindles, we propose that sliding forces from the bridging fiber facilitate kinetochore positioning at the spindle equator (**Fig. 6 A**). We have shown that bridging microtubules slide apart, which is most likely driven by forces generated by motor proteins acting within the antiparallel overlap zones of bridging microtubules. One of these sliding motors is CENP-E based on our finding that its depletion leads to slower poleward flux of bridging microtubules.

The forces from the bridging fiber are transmitted to k-fibers through NuMa and similar proteins that crosslink kinetochore and bridging microtubules. When NuMa is depleted, this transmission is impaired and the k-fiber flux slows down, whereas the bridging fiber flux remains unchanged.

The length of the region of the antiparallel overlap of bridging microtubules is regulated by Kif18A and to a smaller extent Kif4A. This length is especially important because if overlaps between bridging microtubules are longer, then the antiparallel overlap zones between bridging and kinetochore microtubules are also longer, accumulate more motors that slide kinetochore microtubules with respect to the antiparallel bridging microtubules, thereby increasing the flux velocity of the k-fiber (**Fig. 6 B**). This picture is based on our finding that when Kif18A is depleted alone or together with Kif4A and/or PRC1, the overlap zones are longer and the k-fiber flux is equal to the bridging fiber flux.

How can sliding of bridging microtubules promote kinetochore centering? If a pair of kinetochores is misaligned, i.e., displaced towards one pole, then the k-fiber extending towards that pole is shorter than the opposite one and has a shorter overlap with the associated bridging microtubules, both those that extend from the same and from the opposite spindle half. This means that the transmission of the sliding forces from the bridging microtubules to the kinetochore microtubules is less efficient,

causing this short k-fiber to slip along the bridging fiber and flux slower than the bridging fiber. In contrast, the k-fiber on the other side is longer and has a long overlap region with the bridging microtubules, including both those that originate from the same and from the opposite spindle half. Thus, the force transmission to the k-fiber is more efficient and this k-fiber fluxes at a velocity similar to the bridging fiber. Faster flux of the longer k-fiber results in the movement of the midpoint between the two k-fibers in the direction of the longer k-fiber, thereby promoting centering of the kinetochores (**Fig. 6 A**).

We propose that this mechanism based on relative sliding of kinetochore and bridging microtubules works together with the known length-dependent regulation of microtubule dynamics by Kif18A to ensure alignment of kinetochores at the equatorial plane of the spindle in metaphase. This mechanism may also work during prometaphase to promote chromosome movement from polar regions of the spindle towards the equator and their congression at the metaphase plate.

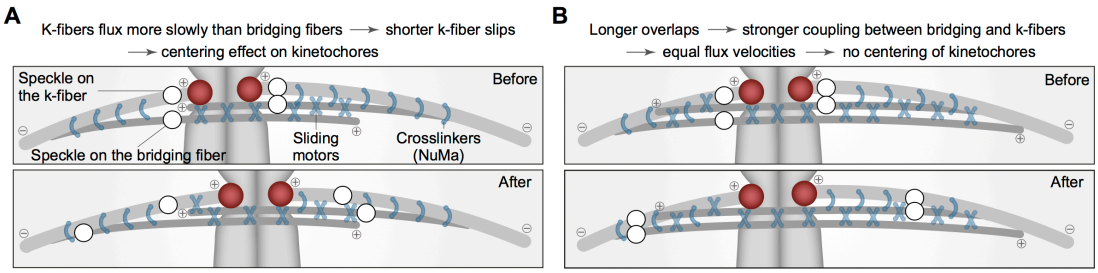

Figure 6. A model for how sliding forces exerted by the bridging fiber onto the sister kinetochore fibers help center the kinetochores on the spindle.
(**A**) The schemes depict how lateral forces acting along the k-fiber help kinetochore alignment at the spindle center. Top: A pair of kinetochores (red circles) is displaced towards the left pole. To visualize relative movements of the microtubules, four marks representing tubulin speckles are denoted, two on k-fibers and two on the antiparallel microtubules of the bridging fiber adjacent to the speckles on the k-fiber (white circles; plus and minus signs mark microtubule ends). Bottom: Over time, the speckles on the bridging fiber move poleward by a similar distance, due to sliding of bridging microtubules driven by motor proteins (blue X-shapes). These sliding forces are transmitted to the k-fibers through crosslinks between the fibers (blue C-shapes), but k-fibers flux more slowly than bridging fibers due to imperfect coupling. In particular, the longer k-fiber on the right side has a longer overlap with the bridging fiber and thus the coupling is stronger, leading to a higher flux velocity of this fiber in comparison with the shorter k-fiber. Thus, the midpoint between the marks on the sister k-fibers, and hence also the kinetochores, move towards the spindle center. We propose that this centering mechanism acts together with the mechanisms that regulate k-fiber plus-end dynamics (not depicted) to drive chromosome alignment.
(**B**) If the coupling between the k-fibers and the bridging fiber is too strong, such as in cases when the antiparallel overlap is excessively long, the k-fibers flux at the same velocity as bridging fibers. In this situation, the sliding forces do not promote kinetochore movement towards the spindle center, resulting in chromosome misalignment.

METHODS

Theory for kinetochore centering

The model describes a system consisting of two sister kinetochores, two microtubules representing the left and the right k-fiber, which extend from the spindle edges to the kinetochores, and two bridging microtubules which extend from the edges and interdigitate in the middle (**Fig. 1 A**). The positions of the sister kinetochores are denoted by $x_{kc}^{\pm}$, while the positions of k-fibers and bridging fibers are taken as arbitrary positions along their lattice and are denoted by $x_{kf}^{\pm}$ and $x_{br}^{\pm}$, respectively. Hereon the superscripts $+$ and $-$ denote the right and left sides of the model, respectively. The connection between the kinetochores is modeled as an elastic spring with elastic coefficient k. The length of the microtubule overlap within the bridging fiber is denoted by D_{br}. Positions of minus ends, $x_p^{\pm}$, are constant in time.

The movement of the kinetochore at time t is calculated from a balance of the elastic force of the spring, given by Hooke's law $F_{el} = k(x_{kc}^{+} - x_{kc}^{-} - x_0)$, where x_0 is the spring rest length, and the force exerted on the kinetochore by the microtubule $F_{kc}^{\pm}$. The balance of those forces is given as

$$F_{kc}^{\pm} = \pm F_{el}. \tag{1}$$

The force exerted on the kinetochore by the microtubule, which depends on the velocity on the kinetochore with respect to the k-fiber lattice, is described by a linear relation, $F_{kc}^{\pm} = -\mu_{kc}(v_{kc}^{\pm} - v_{kf}^{\pm})$, where μ_{kc} denotes the effective friction coefficient at the kinetochore. This description is a simplification of the force-velocity relationship measured for kinetochores (Akiyoshi et al., 2010). From equation (1) it directly follows that forces on sister kinetochores are in balance, $F_{kc}^{+} = -F_{kc}^{-}$. Velocities are calculated as time derivatives of their respective positions: $v_i^{\pm} = \frac{dx_i^{\pm}}{dt}$, where $i =$ kc, kf, br.

The movement of the k-fiber is driven by forces exerted by molecular motors distributed along the k-fiber and bridging microtubule overlap, $F_m^{\pm}$, and at the kinetochore, whereas its sliding with respect to the bridging fiber is damped by the passive cross-linking proteins,

$$F_c^{\pm} + F_m^{\pm} - F_{kc}^{\pm} = 0. \tag{2}$$

The damping force of the cross-linking proteins is given as $F_c^{\pm} = -N_c^{\pm}\mu_c(v_{kf}^{\pm} - v_{br}^{\pm})$, where $N_c^{\pm} = n_c L^{\pm}$ is the number of passive cross-linkers distributed along the parallel overlap of a k-fiber and a bridging fiber and is calculated from linear density n_c and the length of the k-fiber $L^{\pm}=\pm(x_p^{\pm} - x_{kc}^{\pm})$. The parameter μ_c represents the friction coefficient of a cross-linking protein. The forces of the motors distributed along the antiparallel overlap of a k-fiber and a bridging fiber depend on the velocity of the k-fiber in respect to the velocity of the bridging fiber and are given through a linear force-velocity relation $F_m^{\pm} = N_m^{\pm} f_m \left(\pm 1 - \frac{v_{kf}^{\pm} - v_{br}^{\mp}}{v_m}\right)$, where f_m denotes the stall force and v_m the velocity without a load. The number of motors is given by $N_m^{\pm}=n_m D^{\pm}$,

where n_m is the linear density of the motors and $D^{\pm} = \left(\frac{D_{br}}{2} \mp x_{kc}^{\pm}\right) \theta\left(\frac{D_{br}}{2} \mp x_{kc}^{\pm}\right)$ is the length of the antiparallel overlap of the bridging and k-fiber, in which θ is the Heaviside step function which ensures that the antiparallel overlap exists.

The movement of the bridging microtubules is driven by the force exerted by motors distributed along the antiparallel overlap of bridging microtubules, F_{br}, and along the antiparallel overlap of the bridging fiber and the k-fiber. These forces are balanced by the friction that occurs when the bridging fibers slide with respect to the k-fibers,

$$F_c^{\pm} \pm F_{br} - F_m^{\mp} = 0. \tag{3}$$

The force exerted in the overlap of bridging microtubules depends on their relative velocities, $F_{br} = N_{br} f_m \left(1 - \frac{v_{br}^{+} - v_{br}^{-}}{v_m}\right)$, and the number of motors in the overlap of bridging microtubules is given as $N_{br} = n_m D_{br}$.

Solution of the model

Approximations in the model. Even though the model can be solved as given, we introduce two approximations that apply, to a large extent, to the studied spindles. First, we neglect the difference in kinetochore velocities, $v_{kc}^{+} - v_{kc}^{-} = 0$, based on the following arguments. Interkinetochore velocity on a time scale relevant for centering of kinetochores t_c has an approximate value $\Delta v_{kc} \approx (x_{kc}^{+} - x_{kc}^{-})/t_c$. By applying equation (1) on the left and right sides the interkinetochore velocity, related to the difference in k-fiber velocities, reads $\Delta v_{kc} \approx (v_{kf}^{+} - v_{kf}^{-})/(2kt_c/\mu_{kc} + 1)$. In the limit $2kt_c/\mu_{kc} \gg 1$ the interkinetochore velocity approaches zero. This is indeed the case for relevant parameters: spring constant representing elasticity of the chromosomes, $k = 100$ pN/μm (Joglekar and Hunt, 2002), typical time scale of this process, t_c =2 min (Stumpff et al., 2008), and $\mu_{kc} = 30$ pNmin/μm from table in Figure 1C.

Second, we set the velocities of the bridging microtubules to the value $v_{br}^{\pm} = \pm v_m/2$, based on the following calculation. From equation (3) we derive an expression for kinetochores in the central position:

$$\frac{2v_{br}^{+}}{v_m}\left(1 + \frac{N_c^{+}\mu_c}{N_{br} f_m}\frac{v_m}{2} + \frac{D^{-}}{2D_{br}}\right) = 1 + \frac{N_c^{+}\mu_c}{N_{br} f_m} v_{kf}^{+} - \frac{D^{-}}{D_{br}}\left(-1 - \frac{v_{kf}^{-}}{v_m}\right). \tag{4}$$

In the case where the contribution of the motors dominates over that of cross-linkers, $N_c^{+}\mu_c v_m \ll 2N_{br} f_m$, the second term in the bracket on the left side of the equation is much smaller than 1. Analogously, the second term on the right side can be neglected. Because the length of the antiparallel overlap between bridging and k-fibers is much smaller than the length of the overlap between bridging fibers, $D^{-} \ll D_{br}$, the third terms on both sides of the equation can be neglected. In this limit, Eq. (4) reduces to $2v_{br}^{+}/v_m = 1$.

Velocities of k-fibers and kinetochores. By combining the force balance on sister kinetochores with equation (2), we obtain a balance of forces between left and right k-fibers, which are exerted by motors and cross-linkers:

$$F_c^+ + F_m^+ = -F_c^- - F_m^- \tag{5}$$

To have shorter notations in our model, we define three quantities: $\alpha^\pm \equiv (N_c^\pm \mu_c + N_m^\pm f_m/v_m + \mu_{kc})^{-1}$, $g_c^\pm N_c^\pm \mu_c$, and $g_m^\pm \equiv N_m^\pm f_m/v_m$. These quantities do not depend on velocities of k-fibers and kinetochores, but only on the geometry of the system. Next, by using approximations, described in the previous subsection, and force-velocity relationships on equation (2) for the right and left side of the model we derive expressions for k-fiber velocities:

$$v_{kf}^\pm = \alpha^\pm \left(\mu_{kc} v_{kc} \pm \frac{v_m}{2} \left(g_c^\pm + g_m^\pm \right) \right) \tag{6}$$

In this equation k-fiber velocities for the left and right sides separate, but they depend on the velocity of kinetochores. By applying force-velocity relationships on equation (5) and combining it with equation (6) we obtain a final expression for kinetochore velocities:

$$v_{kc} = \frac{v_m}{2\mu_{kc}} \frac{\left(g_c^+ + g_m^+\right)\left(1 - \alpha^+\left(g_c^+ + g_m^+\right)\right) - \left(g_c^- + g_m^-\right)\left(1 - \alpha^-\left(g_c^- + g_m^-\right)\right)}{\alpha^+\left(g_c^+ + g_m^+\right) + \alpha^-\left(g_c^- + g_m^-\right)} \tag{7}$$

This expression depends explicitly only on the geometry of the system. Thus, the positions of kinetochores can be calculated directly by integrating equation (7).

To calculate kinetochore velocity in the vicinity of the center we solve equation (7) for small displacements, while keeping only the terms linear to the displacement. For a displacement from center, Δx, we can write $g_c^\pm = n_c \mu_c (L_0 \pm \Delta x)$ and $g_m^\pm = n_m f_m / v_m (\mathrm{D}_0 \pm \Delta x)$. Here L_0 denotes the length of k-fibers and D_0 denotes the length of the antiparallel overlap between bridging and k- fibers, for centered kinetochores. By keeping only the terms that are linear in Δx, equation (7) reads:

$$v_{kc} = \frac{v_m}{2} \frac{n_m f_m / v_m + n_c \mu_c}{\mathrm{D}_0 n_m f_m / v_m + L_0 n_c \mu_c} \left(1 + \mathrm{D}_0 \frac{n_m f_m}{\mu_{kc} v_m} + L_0 \frac{n_c \mu_c}{\mu_{kc}} \right)^{-1} \Delta x. \tag{8}$$

We can also write this expression as $v_{kc} = \Delta x / T$, where T is characteristic centering time of the kinetochores and is given as in Figure 1C.

Choice of parameters

The value for the stall force of sliding motors f_m was taken from literature (Valentine et al., 2006) and the value for the sliding motor velocity without a load v_m was set to reproduce the measured velocity of the bridging microtubule and has similar value to the microtubule sliding velocity that is driven by Eg5 motor proteins from *Xenopus laevis* (Hentrich and Surrey, 2010). The value for the effective friction coefficient μ_{kc} is estimated as a ratio of the stall force at the kinetochore, which is 3 pN (Akiyoshi et al., 2010) and the polymerization velocity measured here, 0.1 μm/min. Two independent parameters, sliding motor density n_m and passive cross-linker friction multiplied by its density $n_c \mu_c$, were considered as variable parameters and were varied

over two orders of magnitude in order to explore parameter space. Values for geometrical parameters, k-fiber length L_0 and overlap length D_0, were measured in this experiment.

Exploration of parameter space

The characteristic centering time is explored for most relevant biological parameters in Figure 1. Here, we systematically explore the parameter space by varying the values of all unknown biological parameters, density of sliding motors, density of cross-linking proteins and the effective friction coefficient (n_m, n_c, μ_{kc}), as well as geometrical parameters, k-fiber length and overlap length (L_0, D_0).

By varying the densities of sliding motors and cross-linkers, we find that the centering mechanism has an optimal regime, characterized by a minimum in centering time, when the density of cross-linkers is kept constant (**Fig. S1 A**). From this plot we also see that biologically relevant characteristic centering time, which is less than 4 minutes, can be achieved for a wide range of parameter values, suggesting that this centering mechanism is efficient regardless of variability in biological systems.

Varying the cross-linker density and bridging and k- fiber overlap length at the same time, we find that the minimum in centering time is reached when both parameters approach zero (**Fig. S1 B**). The increase of centering time for variations in both parameters appears to be roughly linear, and the lines depicting areas of same centering time are almost straight.

We also explore the changes in characteristic centering time when varying both the effective friction coefficient at the kinetochores and the motor density (**Fig. S1 C**). We find that the effective friction at the kinetochores plays an important role in the centering mechanism, because biologically relevant centering time can be achieved for larger values of this parameter. We also observe that the increase in centering time caused by the increase in motor density can be compensated by the increase in effective friction at the kinetochores.

Experimental Methods

Cell culture

hTERT-RPE-1 cell line with a stable expression of CENP-A-GFP and centrin1-GFP was a gift from Alexey Khodjakov (Wadsworth Center, New York State Department of Health, Albany, NY, USA) (developed in (Magidson et al., 2011). Cells were maintained in Dulbecco's Modified Eagle's Medium (containing 1 g/L d-glucose, l-glutamine, pyruvate; Lonza, Basel, Switzerland) supplemented with 10% Fetal Bovine Serum (Sigma-Aldrich, St. Louis, MO, USA), 100 IU/mL penicilin (Lonza) and 100 mg/mL streptomycin (Lonza). Cells were grown at 37 ºC in a Galaxy 170s humidified incubator (Eppendorf) with a 5% CO2 atmosphere.

RNA interference and transfection

One day before transfection, 120 000 cells were seeded on 35-mm glass coverslip dishes with 0.17-mm glass thickness (MatTek Corporation). siRNA constructs were diluted in Opti-MEM medium (Life Technologies) and transfection was performed with Lipofectamine RNAiMAX Reagent (Life Technologies) by following manufacturer's protocol. Constructs and their final concentrations used were: 100 nM NuMA siRNA (sc-43978; Santa Cruz Biotechnology), 300 nM PRC1 siRNA (L-019491-00-0010; Dharmacon), 100 nM Ndc80 siRNA (HA12977117-004; Merck), 20 nM Haus8 siRNA (L-031247-01-0005; Dharmacon), 100 nM CENP-E siRNA (L-003252-000010; Dharmacon), 100 nM Kif4A siRNA (sc-60889; Santa Cruz Biotechnology) and 100 nM Kif18A siRNA (4390825; Ambion). After 4 h of incubation with transfection mixure, medium was replaced with regular cell culture medium. All experiments on siRNA-treated cells were perfomed 24 h after transfection, except for Haus8 siRNA-depleted cells, where silencing was done for 48 h. All treatments include at least three independent experiments.

Speckle microscopy

Cells grown in glass coverslip dishes were stained with 1 nM SiR-tubulin dye (Spirochrome AG). After 15 min of staining, live imaging was performed on a spinning disk confocal microscope system (Dragonfly; Andor Technology) using 63x/1.47 HC PL APO glycerol objective (Leica) and Zyla 4.2P scientific complementary metal oxide semiconductor (sCMOS) camera (Andor Technology). During imaging, cells were maintained at 37 ºC and 5% CO2 within H301-T heating chamber (Okolab). Images were acquired using Fusion software (v 2.2.0.38).
For live imaging of RPE1 cells expressing CENP-A-GFP and centrin1-GFP, and stained with SiR-tubulin, 488-nm and 561-nm laser lines were used to excitate GFP, and SiR, respectively. In order to visualize SiR-tubulin speckles, images were acquired with 80% laser power and exposure of 1 s. Image acquisition was done on one focal plane every 10 s. Note that time-frame within which SiR-tubulin, at 1 nM concenration, can be visualized in patches on the mitotic spindle is between 15 and 75 min after SiR-tubulin staining.

Immunostaining

Cells were fixed in ice-cold methanol for 1 min and permeabilized for 15 min in 0.5% Triton X-100 in PBS. Following permeabilization, cells were blocked with 1% NGS in PBS for 1 h and incubated with primary antibodies at 4 ºC overnight. Primary antibodies were prepared in 1% NGS in PBS to 1:100 dilution. Following incubation with primary antibodies, cells were incubated with fluorescence-conjugated secondary antibodies at room temperature for 1 h. Secondary antibodies were prepared in 2% NGS in PBS to 1:250 dilution. To visualize DNA, cells were stained with DAPI for 10 min. After each step, cells were washed three times in PBS for 5 min. Primary

antibodies used were: mouse anti-NuMa (sc-365532; Santa Cruz Biotechnology), mouse anti-PRC1 (sc-376983; Santa Cruz Biotechnology), rabbit anti-CENP-E (C7488; Sigma-Aldrich), mouse anti-Kif4A (sc-365144; Santa Cruz Biotechnology), and rabbit anti-Kif18A (A301-080A; Bethyl Laboratories). Secondary antibodies used were: donkey anti-mouse IgG-Alexa 594 (Abcam), donkey anti-rabbit IgG-Alexa 594 (Abcam), and donkey anti-rabbit IgG-Alexa 647 (Abcam). Immunostained cells were imaged using Bruker Opterra Multipoint Scanning Confocal Microscope (Bruker Nano Surfaces) with a Nikon CFI Plan Apo VC 100x/1.4 numerical aperture oil objective (Nikon). 405/488/561/640-nm laser lights were used with following emission filters: BL HC 525/30, BL HC 600/37 and BL HC 673/11 (Semrock). Images were captured with an Evolve 512 Delta Electron Multiplying Charge Coupled Device (EMCCD) Camera (Photometrics) using a 200 ms exposure time.

Image analysis

Measurements were performed in Fiji/ImageJ (National Institutes of Health). Quantification and data analysis were performed in R (R Foundation for Statistical Computing) and MATLAB (MathWorks). Figures and schemes were assembled in Adobe Illustrator CC (Adobe Systems). Statistical analysis was performed using Student's t-test and Mann-Whitney test.

Upon inspection of tubulin speckle movement within the spindle, speckles which could be followed in at least four time frames were taken into account. For every tubulin speckle position, corresponding CENP-A and centrin positions, suggestive of the location of sister kinetochores and spindle poles, respectively, were also tracked. Tracking was done by using *Multi-point* tool. Speckles which started at proximal kinetochore were categorized as part of k-fiber, whilst speckles which started between sister kinetochores or proximal to the distal pole and passed through sister kinetochores were categorized as part of bridging fiber. Speckles which could not be categorized as part of k-fiber or bridging fiber are termed other. Speckle-pole velocity was calculated by fitting linear regression on distances between tubulin speckle and spindle pole towards which speckle is moving to during first 30 s of its trajectory. Similar was done to determine speckle-kinetochore velocity, however, distances between tubulin speckle and proximal sister kinetochore were used. Speckles were categorized as part of the leading k-fiber when moving in the same direction as sister kinetochores or trailing when moving in the opposite direction.

For kinetochore alignment and inter-kinetochore distance measurements, *Multipoint* tool was used to track positions of sister kinetochore pairs. The equatorial plane was defined with two points placed between outermost pairs of kinetochores on the opposite sides of the spindle. Kinetochore alignment was calculated as the distance between the midpoint of kinetochore pairs and equatorial plane, while inter-kinetochore distance as the distance between two sister kinetochores.

In cells immunostained for PRC1, 5-pixel-thick segmented line was used to track the pole-to-pole contour of PRC1-labeled overlap region. The pole-to-pole tracking was performed on single z-planes and the mean value of the cytoplasm was subtracted

from the retrieved intensity profiles. The overlap length was determined as the width of the peak of the signal intensity in the central part of the contour in SciDavis (Free Software Foundation Inc.). The width of the peak was measured at the base of the PRC1 intensity peak where the PRC1 signal is roughly equal to the mean value of the PRC1 signal along the contour on either side of the peak.
To determine percentage of protein depletion, we measured mean spindle intensity by encompassing the area of the spindle with *Polygon selection* tool. Mean background intensity in the cytoplasm, measured using 1x1 μm rectangle, was subtracted from mean spindle intensity.

ACKNOWLEDGEMENTS

We thank Alexey Khodjakov for the hTERT-RPE1 CENP-A-GFP Centrin1-GFP cell line, Ivana Šarić for the drawings, and all members of Tolić and Pavin groups for helpful discussions. This work was funded by the European Research Council (ERC Consolidator Grant, GA Number 647077, granted to I.M.T.), the Croatian Science Foundation (HRZZ, project IP-2014-4753, granted to I.M.T.), and the QuantiXLie Center of Excellence, a project co-financed by the Croatian Government and European Union through the European Regional Development Fund—the Competitiveness and Cohesion Operational Programme (Grant KK.01.1.1.01.0004). We also acknowledge new support by the ERC (Synergy Grant, GA Number 855158, granted to I.M.T.). The work of the doctoral student M.J. has been supported by the "Young researchers' career development project – training of doctoral students" of the Croatian Science Foundation.

AUTHOR CONTRIBUTIONS

P.R. and M.J. performed all experiments. P.R. analyzed the data with help of M.J. D.B. developed the model, based on A.B's pilot work. N.P. and I.M.T. conceived the project and supervised the theory and experiments.

References

Akiyoshi, B., K.K. Sarangapani, A.F. Powers, C.R. Nelson, S.L. Reichow, H. Arellano-Santoyo, T. Gonen, J.A. Ranish, C.L. Asbury, and S. Biggins. 2010. Tension directly stabilizes reconstituted kinetochore-microtubule attachments. *Nature*. 468:576-579.

Armond, J.W., E.F. Harry, A.D. McAinsh, and N.J. Burroughs. 2015. Inferring the Forces Controlling Metaphase Kinetochore Oscillations by Reverse Engineering System Dynamics. *PLoS Comput. Biol.* 11:e1004607.

Bieling, P., I. Kronja, and T. Surrey. 2010a. Microtubule motility on reconstituted meiotic chromatin. *Curr Biol*. 20:763-769.

Bieling, P., I.A. Telley, and T. Surrey. 2010b. A minimal midzone protein module controls formation and length of antiparallel microtubule overlaps. *Cell*. 142:420-432.

Bringmann, H., G. Skiniotis, A. Spilker, S. Kandels-Lewis, I. Vernos, and T. Surrey. 2004. A kinesin-like motor inhibits microtubule dynamic instability. *Science*. 303:1519-1522.

Brouhard, G.J., and A.J. Hunt. 2005. Microtubule movements on the arms of mitotic chromosomes: polar ejection forces quantified in vitro. *Proc Natl Acad Sci U S A*. 102:13903-13908.

Cheeseman, I.M., J.S. Chappie, E.M. Wilson-Kubalek, and A. Desai. 2006. The conserved KMN network constitutes the core microtubule-binding site of the kinetochore. *Cell*. 127:983-997.

Cheeseman, I.M., and A. Desai. 2008. Molecular architecture of the kinetochore-microtubule interface. *Nature reviews. Molecular cell biology*. 9:33-46.

David, A.F., P. Roudot, W.R. Legant, E. Betzig, G. Danuser, and D.W. Gerlich. 2019. Augmin accumulation on long-lived microtubules drives amplification and kinetochore-directed growth. *The Journal of cell biology*. 218:2150-2168.

Du, Y., C.A. English, and R. Ohi. 2010. The kinesin-8 Kif18A dampens microtubule plus-end dynamics. *Curr Biol*. 20:374-380.

Dudka, D., A. Noatynska, C.A. Smith, N. Liaudet, A.D. McAinsh, and P. Meraldi. 2018. Complete microtubule-kinetochore occupancy favours the segregation of merotelic attachments. *Nature communications*. 9:2042.

Elting, M.W., M. Prakash, D.B. Udy, and S. Dumont. 2017. Mapping Load-Bearing in the Mammalian Spindle Reveals Local Kinetochore Fiber Anchorage that Provides Mechanical Isolation and Redundancy. *Curr. Biol.* 27:2112-2122.

Fonseca, C.L., H.L.H. Malaby, L.A. Sepaniac, W. Martin, C. Byers, A. Czechanski, D. Messinger, M. Tang, R. Ohi, L.G. Reinholdt, and J. Stumpff. 2019. Mitotic chromosome alignment ensures mitotic fidelity by promoting interchromosomal compaction during anaphase. *The Journal of cell biology*. 218:1148-1163.

Forer, A. 1965. Local reduction of spindle fiber birefringence in living Nephrotoma suturalis (Loew) spermatocytes induced by ultraviolet microbeam irradiation. *The Journal of cell biology*. 25:Suppl:95-117.

Ganem, N.J., K. Upton, and D.A. Compton. 2005. Efficient mitosis in human cells lacking poleward microtubule flux. *Curr Biol*. 15:1827-1832.

Garcia, M.A., N. Koonrugsa, and T. Toda. 2002. Two kinesin-like Kin I family proteins in fission yeast regulate the establishment of metaphase and the onset of anaphase A. *Curr Biol*. 12:610-621.

Goshima, G., M. Mayer, N. Zhang, N. Stuurman, and R.D. Vale. 2008. Augmin: a protein complex required for centrosome-independent microtubule generation within the spindle. *The Journal of cell biology*. 181:421-429.

Gruneberg, U., R. Neef, X. Li, E.H. Chan, R.B. Chalamalasetty, E.A. Nigg, and F.A. Barr. 2006. KIF14 and citron kinase act together to promote efficient cytokinesis. *J. Cell Biol.* 172:363-372.

Hamaguchi, Y., M. Toriyama, H. Sakai, and Y. Hiramoto. 1987. Redistribution of fluorescently labeled tubulin in the mitotic apparatus of sand dollar eggs and the effects of taxol. *Cell Struct Funct*. 12:43-52.

Hentrich, C., and T. Surrey. 2010. Microtubule organization by the antagonistic mitotic motors kinesin-5 and kinesin-14. *The Journal of cell biology*. 189:465-480.

Hiramoto, Y., and K. Izutsu. 1977. Poleward movement of "markers" existing in mitotic spindles of grasshopper spermatocytes. *Cell Structure and Function*. 2:257-259.

Jagrić, M., P. Risteski, J. Martinčić, A. Milas, and I.M. Tolić. 2021. Optogenetic control of PRC1 reveals its role in chromosome alignment on the spindle by overlap length-dependent forces. *eLife*. 10:e61170.

Joglekar, A.P., and A.J. Hunt. 2002. A simple, mechanistic model for directional instability during mitotic chromosome movements. *Biophysical journal*. 83:42-58.

Kajtez, J., A. Solomatina, M. Novak, B. Polak, K. Vukusic, J. Rudiger, G. Cojoc, A. Milas, I. Sumanovac Sestak, P. Risteski, F. Tavano, A.H. Klemm, E. Roscioli, J. Welburn, D. Cimini, M. Gluncic, N. Pavin, and I.M. Tolic. 2016. Overlap microtubules link sister k-fibres and balance the forces on bi-oriented kinetochores. *Nature communications*. 7:10298.

Kamasaki, T., E. O'Toole, S. Kita, M. Osumi, J. Usukura, J.R. McIntosh, and G. Goshima. 2013. Augmin-dependent microtubule nucleation at microtubule walls in the spindle. *The Journal of cell biology*. 202:25-33.

Levesque, A.A., and D.A. Compton. 2001. The chromokinesin Kid is necessary for chromosome arm orientation and oscillation, but not congression, on mitotic spindles. *The Journal of cell biology*. 154:1135-1146.

Lukinavicius, G., L. Reymond, E. D'Este, A. Masharina, F. Gottfert, H. Ta, A. Guther, M. Fournier, S. Rizzo, H. Waldmann, C. Blaukopf, C. Sommer, D.W. Gerlich, H.D. Arndt, S.W. Hell, and K. Johnsson. 2014. Fluorogenic probes for live-cell imaging of the cytoskeleton. *Nat. Methods*. 11:731-733.

Magidson, V., C.B. O'Connell, J. Loncarek, R. Paul, A. Mogilner, and A. Khodjakov. 2011. The spatial arrangement of chromosomes during prometaphase facilitates spindle assembly. *Cell*. 146:555-567.

Maiato, H., A.M. Gomes, F. Sousa, and M. Barisic. 2017. Mechanisms of Chromosome Congression during Mitosis. *Biology (Basel)*. 6.

Manenica, M., V. Štimac, I. Koprivec, J. Simunić, and I.M. Tolić. 2020. Augmin regulates kinetochore tension and spatial arrangement of spindle microtubules by nucleating bridging fibers. *bioRxiv*.

Mayr, M.I., S. Hummer, J. Bormann, T. Gruner, S. Adio, G. Woehlke, and T.U. Mayer. 2007. The human kinesin Kif18A is a motile microtubule depolymerase essential for chromosome congression. *Curr. Biol*. 17:488-498.

McDonald, K.L., E.T. O'Toole, D.N. Mastronarde, and J.R. McIntosh. 1992. Kinetochore microtubules in PTK cells. *The Journal of cell biology*. 118:369-383.

Mishima, M., S. Kaitna, and M. Glotzer. 2002. Central spindle assembly and cytokinesis require a kinesin-like protein/RhoGAP complex with microtubule bundling activity. *Dev Cell*. 2:41-54.

Mitchison, T.J. 1989. Polewards microtubule flux in the mitotic spindle: evidence from photoactivation of fluorescence. *The Journal of cell biology*. 109:637-652.

O'Toole, E., M. Morphew, and J.R. McIntosh. 2020. Electron tomography reveals aspects of spindle structure important for mechanical stability at metaphase. *Mol Biol Cell*. 31:184-195.

Polak, B., P. Risteski, S. Lesjak, and I.M. Tolic. 2017. PRC1-labeled microtubule bundles and kinetochore pairs show one-to-one association in metaphase. *EMBO Rep*. 18:217-230.

Rogers, G.C., S.L. Rogers, T.A. Schwimmer, S.C. Ems-McClung, C.E. Walczak, R.D. Vale, J.M. Scholey, and D.J. Sharp. 2004. Two mitotic kinesins cooperate to drive sister chromatid separation during anaphase. *Nature*. 427:364-370.

Steblyanko, Y., G. Rajendraprasad, M. Osswald, S. Eibes, A. Jacome, S. Geley, A.J. Pereira, H. Maiato, and M. Barisic. 2020. Microtubule poleward flux in human cells is driven by the coordinated action of four kinesins. *The EMBO journal*:e105432.

Stumpff, J., G. von Dassow, M. Wagenbach, C. Asbury, and L. Wordeman. 2008. The kinesin-8 motor Kif18A suppresses kinetochore movements to control mitotic chromosome alignment. *Dev. Cell*. 14:252-262.

Stumpff, J., M. Wagenbach, A. Franck, C.L. Asbury, and L. Wordeman. 2012. Kif18A and chromokinesins confine centromere movements via microtubule growth suppression and spatial control of kinetochore tension. *Dev. Cell*. 22:1017-1029.

Valentine, M.T., P.M. Fordyce, T.C. Krzysiak, S.P. Gilbert, and S.M. Block. 2006. Individual dimers of the mitotic kinesin motor Eg5 step processively and support substantial loads in vitro. *Nature cell biology*. 8:470-476.

Vladimirou, E., N. McHedlishvili, I. Gasic, J.W. Armond, C.P. Samora, P. Meraldi, and A.D. McAinsh. 2013. Nonautonomous movement of chromosomes in mitosis. *Dev Cell*. 27:60-71.

Vukusic, K., R. Buda, A. Bosilj, A. Milas, N. Pavin, and I.M. Tolic. 2017. Microtubule Sliding within the Bridging Fiber Pushes Kinetochore Fibers Apart to Segregate Chromosomes. *Dev Cell*. 43:11-23 e16.

Vukusic, K., R. Buda, I. Ponjavic, P. Risteski, and I.M. Tolic. 2019. Chromosome segregation is driven by joint microtubule sliding action of kinesins KIF4A and EG5. *bioRxiv*.

Wandke, C., M. Barisic, R. Sigl, V. Rauch, F. Wolf, A.C. Amaro, C.H. Tan, A.J. Pereira, U. Kutay, H. Maiato, P. Meraldi, and S. Geley. 2012. Human chromokinesins promote chromosome congression and spindle microtubule dynamics during mitosis. *J. Cell Biol.* 198:847-863.

Wargacki, M.M., J.C. Tay, E.G. Muller, C.L. Asbury, and T.N. Davis. 2010. Kip3, the yeast kinesin-8, is required for clustering of kinetochores at metaphase. *Cell Cycle*. 9:2581-2588.

Waterman-Storer, C.M., and E.D. Salmon. 1998. How microtubules get fluorescent speckles. *Biophysical journal*. 75:2059-2069.